UConn-40870-0037

MEXICAN ASTROPHYSICAL SUMMER SCHOOL - 1999

LECTURES ON:

PRECISION LABORATORY MEASUREMENTS IN NUCLEAR ASTROPHYSICS [1]

Moshe Gai[2]

Laboratory for Nuclear Science, Department of Physics, U3046

University of Connecticut, 2152 Hillside Rd., Storrs, CT 06269-3046, USA

(gai@uconn.edu; http://www.phys.uconn.edu)

Abstract

After reviewing some of the basic concepts, nomenclatures and parametrizations of Astronomy, Astrophysics, Cosmology, and Nuclear Physics, we introduce a few central problems in Nuclear Astrophysics, including the hot-CNO cycle, helium burning and solar neutrinos. We demonstrate that in this new era of Precision Nuclear Astrophysics **Secondary or Radioactive Nuclear Beams** allow for progress.

Table of Content:

[1]Supported in Part by USDOE Grant No. DE-FG02-94ER40870

[2]Lectures at Mexican Summer School, Aug. 4-11, 1999, Guanajuato, Mexico.

1 INTRODUCTION

In this lecture notes we discuss some aspects of Nuclear Astrophysics and Laboratory measurements of nuclear processes which are of central value for stellar evolution and models of cosmology. These reaction rates are important for several reason. At first they allow us to carry out a quantitative detailed estimate of the formation (and the origin) of the elements; e.g. the origin of ^{11}B *or* ^{19}F . In these cases the understanding of the nuclear processes involved is essential for understanding the origin of these elements. The understanding of the origin of these elements on the other hand, may teach us about exotic processes such as neutrino scattering that may occur in stars and are believed to produce the observed abundances of ^{11}B *and* ^{19}F. More importantly, in most cases details of many astronomical events, such as supernova, are hidden from the eyes of the observer (on earth). In most cases the event is shielded by a large mass and only telltales arrive on earth. Such telltales include neutrinos, or even some form of radiation. One of the most important telltale of an astronomical event are the elements produced by the thermonuclear nucleosynthesis. And in this case it is imperative that we completely understand the nuclear processes so that we can carry out an accurate test of the cosmological or stellar evolution models. In some cases, such as in the solar model, understanding of the nuclear processes in hydrogen burning allow for a test of the standard model of particle physics and a search for phenomena beyond the standard model, such as neutrino masses (neutrino magnetic moment?) or neutrino oscillations. Type 1a supernova on the other hand proved to be a very useful cosmological yard stick allowing for accurate measurements of some of the largest distances of the order of a few Billion Light Years (GLY). Such measurements gave evidence for an accelerating expanding Universe and appear to be one of the most disturbing discovery in Cosmology in recent times. In this case one needs to understand the process of helium burning in a type 1a supernova. In all cases one needs to understand Nuclear reaction rates at energies which are considerably below where they can be measured in the laboratory, and one needs to develop reliable method(s) for extrapolation to low energies.

In spite of concentrated effort by Nuclear Astrophysicists on both experimental and theoretical sides a number of problems remain unsolved, including specific processes in helium and hydrogen burning. In contrast to many cases in Nuclear Astrophysics in the case of the solar neutrinos and type 1a supernovae, the processes of hydrogen burning and helium burning, respectively, must be measured with high precision of the oredr of 5-10%. These problems are in fact central to the field and must be addressed in order to allow for progress. In these lectures we will address these issues and suggest new experiments and new solutions.

Radioactive Nuclear Beams (RNB) now available at many laboratories around the world have already yielded some solutions to problems of current interest, e.g. in the Hot CNO cycle or hydrogen burning, and appear very promising for extending our knowledge to processes in exploding stars, such as the rp process. We will review in this lectures some of the current and future applications of such secondary (radioactive) beams.

In the first section we will define some scales, classifications of stars, nomenclatures, parameters and parametrization of relevance for nuclear astrophysics. We will then review some of the classical reaction chains in burning processes and discuss traditional laboratory measurements of the relevant nuclear reaction rates. In the later part of the lecture series we will develop new ideas for laboratory measurements of the required rates, mostly carried out in the time reversed fashion. We will demonstrate that by measuring the reaction rates in a time reversed fashion we construct a **"Narrow Band Width Hi Fi Amplifier"** that may allow for a measurement of the small cross sections involved. It is important to test whether in fact we construct a "Hi Fidelity Amplifier", so that we are indeed measuring rates relevant for nuclear astrophysics. These new techniques allow us to tackle some of the oldest open questions in Nuclear Astrophysics including the rate for the $^{12}C(\alpha,\gamma)^{16}O$ reaction of helium burning and the $^{7}Be(p,\gamma)^{8}B$ reaction of importance for the solar neutrino problem.

2 SCALES AND CLASSIFICATION OF STARS

Most stars have been around for long time and thus have reached a state of statistical (hydro-dynamical) equilibrium. Indeed most properties of stars arise from simple hydrodynamical consideration or from the fact that stars are nearly (but not perfect) black body radiators. Some of the most obviously required observational parameters of a star are its distance from the earth and its spectrum of light emission and thus its color.

Early studies by Kepler and scientist of the Newtonian era allowed for accurate measurements of the radii and periods of orbital motion of the various planets, including the earth. In these measurements the appearance of comets were very pivotal and indeed the return of Halley's comet in April of 1759, as reported by Harvard astronomers, was announced as a confirmation of Newton's law of gravity. Ironically, when Halley's comet was late to return and did not show up between September 1758 and early April 1759, as predicted by Edmund Halley using Newton's $1/r^2$ law of gravity, Newton's law of gravity was (prematurely) declared wrong [1] by the "skep-

tics". It is also worth noting that while the earliest western record of Halley's comet is from AD 66 (that was linked to the destruction of Jerusalem), the Chinese records go back for another 679 years, as shown in Table 1 [2]. From these measurements of radii and periods, it was possible to determine the mass of the sun and planets with high precision; one solar mass $M_\odot = 1.989 \times 10^{30}$ Kg, and $M_E = 3\mu M_\odot$.

Some of the very early measurements (developed around 1838) of the distance of stars from the earth used the parallax method [3]. It was found that the nearest star, Alpha-Centauri visible in the southern hemisphere (a triple star system composed of Alpha-Centauri Proxima, A and B) produced (after corrections for its angle) 1.52 sec of arc of angular displacement, or a parallax of 0.76 arc sec. Knowing the earth average orbit radius = 149.6 MKm = 1 AU (Astronomical Unit), or approximately 8 light minutes, we calculate 1 parsec $= 3.086 \times 10^{16}$ meter, or 3.262 light years (LY). Indeed our closest neighbor is hopelessly far from us, at a distance of approximately 4.2 LY. Modern days (optical) telescopes have an accuracy of the order of 0.01 sec of an arc and with the use of interferometry one can improve the resolution to 0.001 sec of an arc. Hence, the parallax method has a limited use, for stars closer then 1 kpsc. In Fig. 1, taken from Donald Clayton's book [3], we show characteristic distances and structures in our galaxy. Note that the period of rotation of our galaxy is of the order of 100 million years.

TABLE 1
The Chinese historical Records of the apparition of Halley's Comet

Return	Date		Reign/year	Return	Date		Reign/year
-40	-1057-		The Conquest of Zhou	-20	AD 451		Song Yuanjia 28
	-1056		by Wu-Wang				
-39				-19	530		Liang Zhongdatong 2
-38				-18	607		Sui Daye 3
-37				-17	684		Tang Guangzhai 1
-36				-16	760		Qianyuan 3
-35				-15	837		Kaicheng 2
-34	BC 614		Zhou Qing Wang 5	-14	912		Liang Qianhua 2
-33				-13	989		Song Duangong 2
-32	465		Zhou Zhending Wang 3	-12	1066		Zhiping 3
-31				-11	1145		Shaoxing 15
-30				-10	1222		Jiading 15
-29	240		Qin Wang Zheng 7	-9	1301		Yuan Dade 5
-28	162		Han Wen Di Houyuan 2	-8	1378		Ming Hongwu 11
-27	86		Wu Di Houyan 2	-7	1456		Jingtai 7
-26	11		Yuanyan 2	-6	1531		Jiajing 10
-25	AD 65		Yongping 8	-5	1607		Wanli 35
-24	141		Yonghe 6	-4	1682		Qing Kangxi 21
-23	218		Jianan 23	-3	1759		Qianlong 24
-22	295		Jin Yuankang 5	-2	1835		Daoguang 15
-21	374		Ningkang 2	-1	1910		Xuantong 2

Table 1: Chinese records of Halley's Comet [2].

Early measurements performed on stars also defined its color index [3], using the response of detectors (photographic plates) with band widths spanning the Ultraviolet, Blue and Visual spectra. The color index is defined as Blue magnitude minus the Visual magnitude. Note the magnitude is roughly proportional to -2.5 log(intensity). Hence, hot stars are characterized by small and in fact negative color index while cold stars have large color index. Astronomers are also able to correlate the color index with the (effective) surface temperature of a star, an extensively used parameter in stellar models. Stars are also characterized by their absorption spectra as O, B, A, F, G, K, and M stars (that can be memorized using a non quotable slogan).

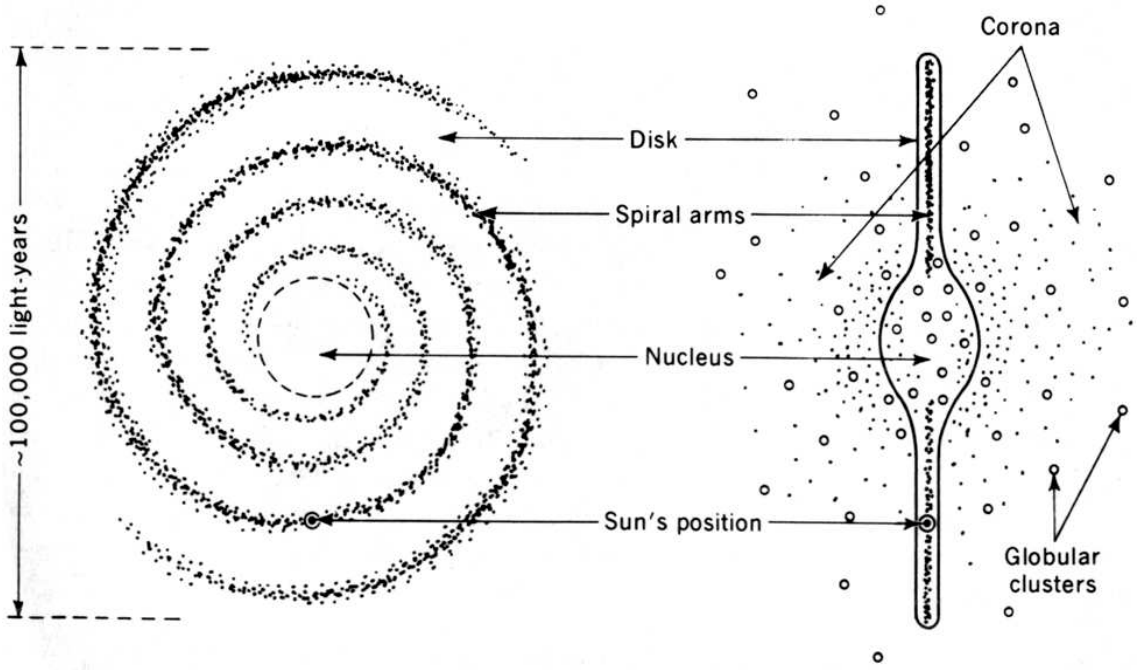

Fig. 1: Scales of our galaxy [3].

2.1 Classification of Stars:

Based on this color index one classify stars using a Hertzsprung-Russell Diagram (after the Danish and American astronomers that developed such diagrams around 1911-1913). In an H-R diagram one plots the Luminosity of a star or the bolometric magnitude (total energy emitted by a star) Vs the surface temperature, or the color index of a star. In Fig. 2 we show such an H-R diagram [3], for star clusters with approximately equal distance to the earth. These stars are believed to be formed within the same time period of approximately 100 million years, which allow for the classification.

Stars that reside on the heavy diagonal curve are referred to as main sequence stars [4]. For the main sequence stars we find the brightest star to be with highest

surface temperature and of blue color. The main sequence stars spend most of their life burning hydrogen and acquire mass that is related to their luminosity: $L = const \times M^{\nu},\ with\ \nu\ =\ 3.5\ to\ 4.0$. Stellar evolution is most adequately described on an H-R diagram, and for example the sun after consuming most of its hydrogen fuel will contract its core while expanding its outer layers (to a radius that will include the earth). The contraction at first raises the luminosity and then the sun will expand and redden, or move up and then to the right in an H-R diagram. At a later stage the helium fuel will ignited in the contracted core and the sun will move to the left on (an asymptotic branch on) the H-R diagram. At the end of helium burning the sun will further contract to a white dwarf, see below, and reside (forever) at the lower bottom left of the H-R diagram. For main sequence stars the luminosity is given by Planck's law $L = 4\pi R^2 \sigma T_e^4$, (we introduced here the effective temperature - T_e, since stars do not have a well defined surface and are not perfect black body radiators). Hence one can determine with limited accuracy the relative radii of main sequence stars. One common way of measuring the radii of stars is by using the interferometry method and the Hanbury-Brown Twiss (HBT) effect [5]. In this measurement one measures the pair correlation function (in momentum space) of two photons and by using boson's statistics one relates the correlation width to the radius (of the source of incoherent photons). For example the sun's radius (not measured via the HBT effect) is $R_\odot = 6.9598 \times 10^8$ meters, or 0.69598 MKm, and $R_E = 1\% R_\odot$. While the average sun's density is $\rho_\odot = 1.4\ g/cm^3$ ($\rho_E = 5.5\ g/cm^3$), the central density of the sun is considerably larger, and it was determined (from stellar hydrodynamical theory of helio-seismological data) to be $\rho = 158\ g/cm^3$ with a central temperature of 15.7 MK [8, 7, 6]. Indeed the gravitational contraction of the sun's central core allows for the heating of the core (from a surface temperature of approximately 6,000 K) and the ignition of the hydrogen burning that occurs at temperatures of a few MK. The convective zone of the sun terminates at a radius of approximately 74% at a temperature of approximately 2 MK and density of approximately $0.12\ g/cm^3$.

Above and to the right of the main sequence stars we find the **Red Giant** stars that are characterized by large luminosity and therefore they are easily seen in the sky. This class includes only a small number of stars, a few percent of the known stars. The redness of these stars arises from their large radii and they represent a star in its later stages of evolution, after it consumed its hydrogen fuel in the core and consist mainly of helium. The subgiant are believed to be stars that expand their outer envelope while contracting their helium cores, leading to the burning of helium. The horizontal branch stars, on the other hand, are believed to be at various stages of helium burning. The supergiant stars are believed to be stars at the advance stages

of their stellar evolution and perhaps approaching the end of their energy-generating life.

In the lower left corner of the H-R diagram we find the **white dwarfs** representing approximately 10% of known stars, which are very dense stars of mass comparable to a solar mass, with considerably smaller radii, comparable to the earth radius. Due to the small surface area these stars have large surface temperature (blue color) in order to allow them to radiate their luminosity. These group composes of the universe's cemetery of stars that are inactive and simply radiate their pressure energy. The white dwarfs are so dense that the electron degeneracy keeps them from collapsing [9], hence can not have a mass larger then approximately $1.4M_{\odot}$, the Chandrasekhar limit, beyond which the electron degeneracy can not overcome the gravitational collapse. Such massive stars (or cores of massive stars) collapse to a neutron star or a black hole under their own gravitational pressure.

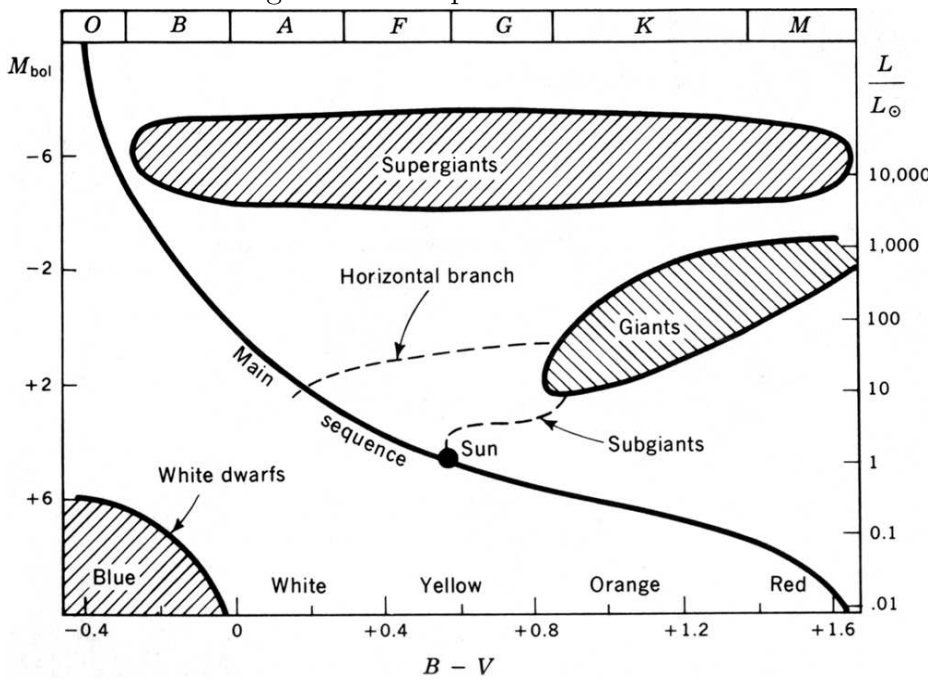

Fig. 2: Hertzsprung-Russell Diagram [3].

Cluster of stars are found very far from the sun, see Fig. 1, and they may contain as many as $10^5 - 10^7$ stars in spherical distribution with a radius in the range of approximately 10 parsec (globular cluster), other clusters include only a few stars. Based on the characteristics of these stars in an H-R diagram it is believed that the age of stars in the globular cluster is of the order of 14 ± 3 billion years (GY) [10], or as old as the universe itself (minus 1 GY). Within this cluster we find a relatively young class with blue giants as the most luminous, called population I, and an older class with red giants as the most luminous members, called population II. The galactic

cluster Pleiades (or Subaru in Japanese) includes its brightest star of blue color, and the M3 globular cluster that includes some 10^5 stars, include its brightest star of red color.

2.2 Age of Stars:

First generation stars are stars that coalesced from the primordial dust that includes approximately 24% helium and 76% hydrogen with traces of lithium. Some of these stars are small enough, and have not evolved and are still burning hydrogen, others already converted to dwarfs. For example the sun (which is not a first generation star) has burned its hydrogen fuel for the last 4.6 Billion years and will do so for approximately 5 more Billion years. Such first generation stars are expected to have very small amount of elements heavier then carbon (some times generically referred to as metals). Thus one defines the metalicity of a star, to be the ratio of its iron (or some time oxygen) to hydrogen content, divided by the metalicity of the sun. This ratio (denoted by square brackets) is usually expressed in a log scale, typically varying between -4 and 0. Stars with metalicity of -3 to -4 are believed to be primordial with ages in the range of 10 to 15 Billion years. It should be emphasized that while the metalicity of a star is measured on its surface, one needs to know the core metalicity and hence one needs to introduce a stellar atmospheric model(s), and thus these data in some cases are model dependent.

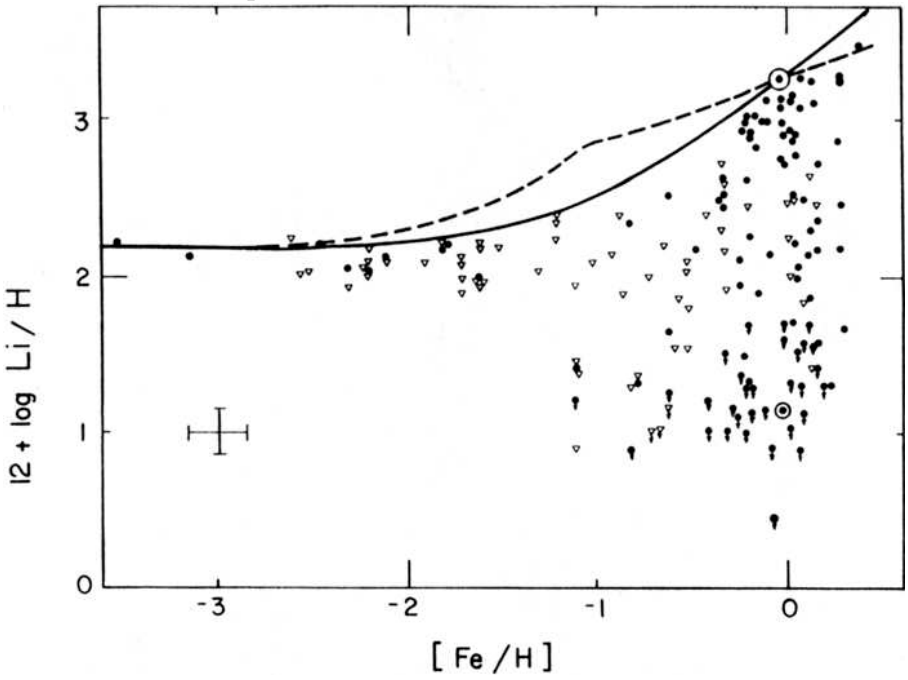

Fig. 3: Lithium abundance Vs metalicity [13].

One of the key questions in cosmology is the primordial abundance of the ele-

ments, produced during the epoch of primordial nucleosynthesis [11, 12]. In Fig. 3 we show the abundance of Li Vs metalicity [13]. Lithium is a very volatile element, since it readily reacts with low energy protons via the $^7Li + p \rightarrow \alpha + \alpha$ reaction, that we depict as $^7Li(p,\alpha)\alpha$. Consequently younger stars show large fluctuations in Li abundance. Fig. 3 includes stars with metalicity as low as -3 and -3.5, and we extrapolate the Li primordial abundance in the range of 10^{-10} *to* 10^{-9}, relative to hydrogen. For younger stars we expect to have an additional lithium roughly proportional to the metalicity. This addition arise from the fact that the inter-stellar gas, from which younger stars coalesce, includes more produced lithium as it exist for longer times. The destruction of lithium in the stellar environment would yield to a depletion in younger stars. Indeed, the measurements of primordial lithium abundance and D and ^3He (first measured on the moon, with the Apollo mission [14]) were very pivotal for confirming Big Bang Nucleosynthesis [11, 12]. In Fig. 4 we show the predicted primordial nucleosynthesis. In these calculations [11] one varies the ratio of photon density to baryon density to yield the observed primordial abundances. And with the knowledge of the photon density, from measurements of the cosmic microwave background, one deduces the baryon density that appears to be less then 10% of the (critical) density required to close the universe. Indeed if one assumes the universe is critically closed (as suggested in inflation models), big bang nucleosynthesis provides some of the strongest evidence for the existence of dark matter in the universe.

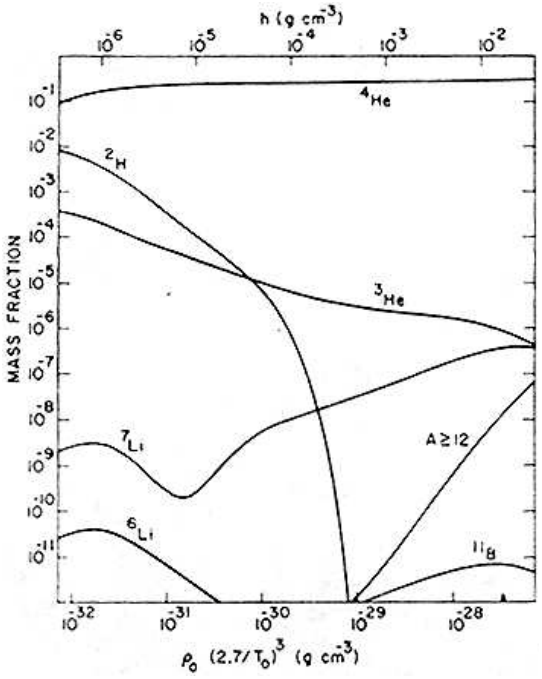

Fig. 4: Big Bang Nucleosynthesis [11].

2.3 Distances to Far Away Stars and Galaxies:

One of the most useful (optical) method to determine the distances of far away stars is with the use of Cepheid Variable stars [3]. These stars undergo periodic variations, which are not necessarily sinusoidal. Sir Edington demonstrated that the pulsation of the Cepheid Variables are due to the transfer of thermal energy of the star to mechanical energy that leads to pulsation [3]. As a consequence the star's period of pulsation is directly related to its mass and its luminosity. Hence, if one measures the apparent luminosity of a Cepheid Variable star (on earth) and its period of pulsation one can infer the distance to the Cepheid Variable and thus the distance of its galactic host.

Type 1a supernova proved to be a very useful and accurate tool in measuring large distances [15]. Type 1a supernova occur in a white dwarf Red Giant binary star system with the white dwarf accumulating hydrogen from the upper stratosphere of the Red Giant. When the white dwarf mass reaches the Chandrasekar limit of 1.4 solar mass, see below, it collapses under its own gravity. The time period of the buildup of light in the light curve of a type 1a supernova (see later Fig. 16), is directly related to its predicted luminosity, and thus measuring the shape of the light curve for type 1a supernova yield its expected luminosity that can be compared to the observed luminosity to yield the distance to the type 1a supernova and its host galaxy. Such modern measurements let us to conclude that the Universe expansion rate is accelerating in recent cosmological times.

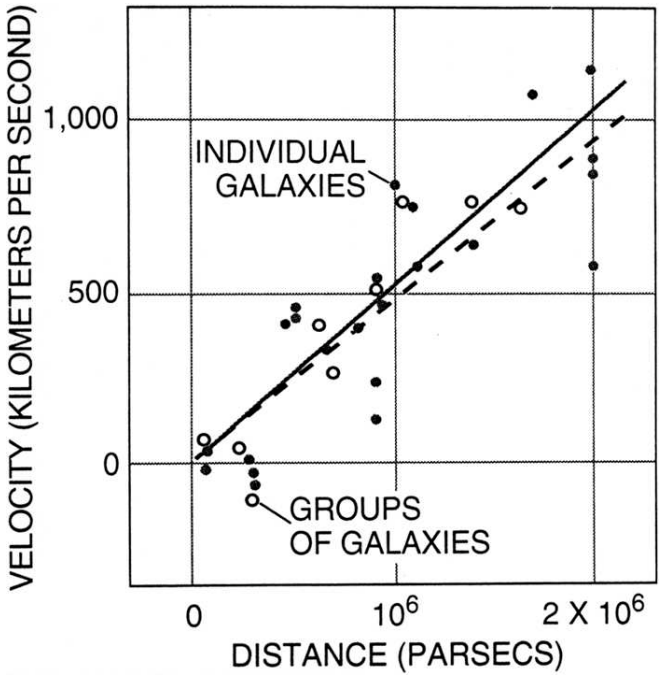

Fig. 5: Hubble's observation of $v = H \times R$ [16].

One of the first uses of the Cepheid variable stars as an astronomical Yard Stick were carried out by Edwin Hubble with the 100 inch telescope at Mt. Wilson observatory near Pasadena, California, during the 1920's [16]. Hubble was able to identify Cepheid Variable stars at a distance of 930,000 LY, and thus well outside our galaxy, of diameter of approximately 100,000 LY (see Fig. 1). Hubble was able to show that these "Faint Nebula" correspond to galaxies different then ours. These nebula were catalogued by Charles Messier in 1781 (with the Crab Nebula being M1) to allow observer to distinguish such objects from comets. Hubble's faint nebula are identified as the M31 (galaxy in Andromeda) and M33 spiral galaxies. Today the distance to the Andromeda nebula is estimated to be over 2 MLY.

Hubble later noticed that the known lines of emission from Hydrogen, Oxygen, Calcium, etc. from stars within the same galaxy are shifted toward the red, which he correctly interpreted as a Doppler shift. Hubble plotted the relative velocity (deduced from the accurate measurement of the redshift) Vs the distance, as he could best estimate using the Cepheid variable. Hubble's original discovery, see Fig. 5, was of a linear relationship between the velocities and distances $v = H \times R$, where H is Hubble's constant. Hubble's measurements of distance were less accurate then possible today, and they yielded the Hubble constant $H = 500\ Km/sec/Mpc$, as can be extracted from Fig. 5.

One of the immediate consequences of Hubble's observation was that it gave credence to the Big Bang hypothesis, developed as one possible solution to Einstein general relativity, in the early 20's by Alexandre Friedman in Russia, and George Lemaitre in Belgium. Details of Big Bang nucleosynthesis were later worked out by de-Sitter and Gamow in the 40's. Incidentally it is suggested that the name Big Bang was coined by Sir Fred Hoyle as a way of ridiculing suggestion of George Lemaitre who referred to his own theory as the theory of the primeval atom. It is ironic that Hoyle who to this date still prefers the steady state theory (and rejects the Big Bang theory), got to name the rival theory. Unfortunately Hubble's determination of H requires a universe that is only 2 Billion Years old. At that time one already knew that the earth and the solar system are much older, of the order of 4.6 Billion years, and the Big Bang theory was rejected. Today due to more accurate determinations of distances (e.g. a factor of 2 change for M31, see above), we believe that the Hubble constant is between 50 to 100 Km/sec/Mpc, with the most probable value at 65, corresponding to a universe between 20 to 10 Billion years old with the most probable age of approximately 14 GY.

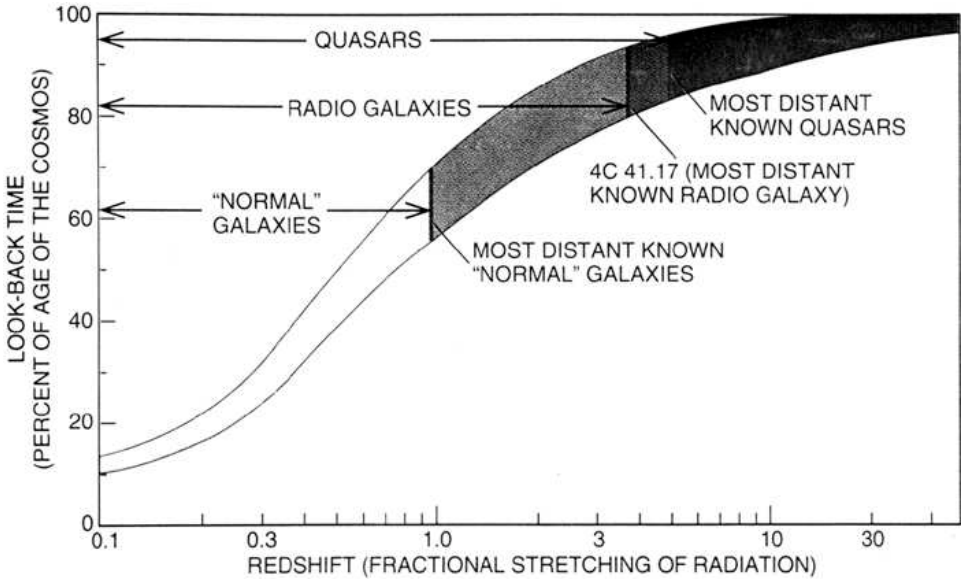

Fig. 6: Look back time VS Red Shift.

The expanding universe allow us to define the Fractional Red-Shift, as the fractional stretching of wave length: $Z = \Delta\lambda/\lambda_0$, with the Doppler shift $\omega = \omega_0\gamma(1+\beta cos\theta)$, and use it to parametrize distances to far away galaxies, radio galaxies, and quasars (young galaxies at the time of formation, mostly composed of gas with luminosity mostly composed of radio electromagnetic radiation). Measurements of these far away objects allow us to look back to the instant of the big bang as shown in Fig. 6, with the oldest known quasar at 5-10% of the age of the universe and the oldest radio galaxy (4C 41.17) at 10-15% of the age of the universe.

2.4 The Big Bang Theory:

The big bang theory most vividly confirmed today by the COBE satellite mission, received one of its first strong confirmations in the work of Arno A. Penzias and Robert W. Wilson in 1964 [17], where they discovered the isotropic emission of microwave radiation from a (cosmological) source at a temperature of approximately 2.7 K. Penzias and Wilson were careful to characterize this thermal source, but did not point to its origin from the expanding universe of the big bang theory. This possibility was in fact pointed out by Peebles and Dicke. Indeed in a preceding paper [18] they demonstrated, that Penzias and Wilson measured the expected microwave remnants of the big bang. In fact Penzias and Wilson who originally only designed an antenna for microwave communication with satellites, first interpreted the continuous hum they detected from all directions of space as arising from pigeon dropping on their antenna.

According to the big bang theory when the Universe was just below 10 μsec,

its temperature was approximately 200 MeV and hence the universe was composed of quarks and gluons solely. At that time a phase transition from the quark gluon plasma to hadron matter occurred. At the age of approximately 1 sec the universe had a temperature of approximately 1 MeV (approximately 10 GK) and then the inverse beta decay process of the neutron to the proton stopped, hence the ratio of neutrons to protons was fixed by the temperature and the mass difference following Boltzmann law. At approximately 100 sec after the big bang when the temperature was approximately 100 keV the epoch of big bang nucleosynthesis commenced [11, 12] and it lasted for a few minutes. During big bang nucleosynthesis as we believe today all the available neutrons were captured to form helium, with a well understood helium fraction of $Y_p = 24\%$. At approximately 300,000 years when the temperature was approximately 10 eV, atoms emerged and accidentaly in the same time the universe became transparent to radiation (decoupling). At this point the universe changed its character from being radiation dominated to matter dominated. As the universe expands all characteristic dimensions expand and radiations from a source of 1 eV (10,000 K) temperature, were redshifted to larger wave lengths of today's observed microwave radiation, corresponding to a source at 2.7 K. Galaxies and stars we believe, first formed when the universe was approximately 1 Billion years old.

Recent speculations suggest that big bang nucleosynthesis may have in fact occurred in an inhomogeneous inflationary universe [19, 20, 21, 22, 23, 24, 25]. This model predicts a low but significantly different, abundance of heavy elements as for example produced in the rapid neutron capture process of supernova [26]. The observation of such heavy elements could test whether the quark-gluon to hadron phase transition is in fact first order. The nature of this phase transition is of great concern for lattice QCD calculations [27] and indeed for understanding QCD. Recent observation of the abundance of ^9Be [28] and ^{11}B, at first appeared promising for this model but subsequent analysis showed that the recently observed abundances (in particular the ratio $^{11}B/^9Be$) are consistent with spallation reaction [29] and no definitive evidence was found for these models of inhomogeneous big bang nucleosynthesis and the standard model of big bang nucleosynthesis prevails.

3 REACTION THEORY, METHODS AND APPLICATIONS

The gravitational pressure in a stellar environment leads to heating of the nuclear fuel. When hydrogen is heated to a temperature in excess of a few MK, it is ignited and nuclear fusion takes place. The fusion of light elements is the source of energy in stars and indeed the most readily available source of energy in the universe today. These fusion reactions aside from "driving stars" are also the origin of the elements heavier then helium. The understanding of thermonuclear processes entails a complete understanding of nuclear reactions as measured in the laboratory, as reviewed by Willie Fowler [30, 31] and the seminal papers of FCZ I [33] and FCZ II [34]. A review of these reactions can also be found in Rolfs and Rodney's book [4]. Usually one would like to know if a reaction rate is sufficiently important to generate the energetic of a stellar environment, and whether it favorably competes with other possible reactions and decays. In this case one needs to define the reaction time scale, or the inverse of its rate, as we discuss below.

Consider two particles a and X, contained in a form of an ideal gas, interacting with each other. The reaction rate per unit volume (r) is given by:

$$r_{ax} = \sigma N_X J_a \tag{1}$$

where σ is the energy dependent cross section, N is the concentration of particles per unit volume, and J is the flux, $J_a = vN_a$, hence:

$$= \sigma v N_X N_a \tag{2}$$

In a star the relative velocities of a and X are distributed in a Maxwell- Boltzmann distribution $\phi(v)$, with $\int \phi(v)dv = 1$, and the total thermonuclear reaction rate is given by:

$$= N_a N_X \int v\sigma(v)\phi(v)dv$$

$$= N_a N_X < \sigma v > \tag{3}$$

and for identical particle we need to introduce a further trivial correction (to avoid double counting):

$$= \frac{N_a N x}{(1+\delta_{aX})} < \sigma v > \tag{4}$$

We define $\lambda = < \sigma v >$, the reaction per unit particle, and equation 4 becomes:

$$r_{aX} = \lambda_{aX} \frac{N_a N x}{(1+\delta_{aX})} \tag{5}$$

We are usually interested in characteristic time scale for the reaction and the time that it takes to remove particle a from the stellar ensemble, which we may want to compare for example to the beta decay lifetime of that particle a, and we define:

$$(\frac{\partial N_X}{\partial t})_a = -\frac{N_X}{\tau_a(X)} \tag{6a}$$

$$= -r_{aX}$$

hence:

$$\tau_a(X) = \frac{1}{\lambda_{aX} N_a}$$

$$= \frac{1}{<\sigma v> N_a} \tag{6}$$

with the correct units of inverse time. Note that the symmetry factor $(1 + \delta_{aX})$ is now on both sides of equation 6a and it drops out. In order to know if a reaction rate competes favorably with a decay rate, one needs to evaluate equ. 6 for that reaction. It is customary to include avogadro's number, $N_A = 6.023 \times 10^{23}$ in equ. 6, and one usually quotes: $N_A < \sigma v > N_a$ and N_a is specified in units of moles/Volume.

Inserting the Maxwellian into the integral in equation 6, we find:

$$< \sigma v > = 4\pi (\frac{\mu}{2\pi k T})^{3/2} \int v^3 \sigma(v) e^{-\frac{\mu v^2}{2kT}} \, dv \tag{7}$$

with μ the reduced mass.

Equations 6 and 7 include information from both nuclear physics (the cross section - σ) and stellar models (the stellar density and temperature). The integral is then the meeting ground for nuclear physics and stellar physics. Clearly the goal of nuclear astrophysics is to evaluate reactions rates relevant to stellar environments, by use of theoretical or experimental methods.

3.1 The S-Factor:

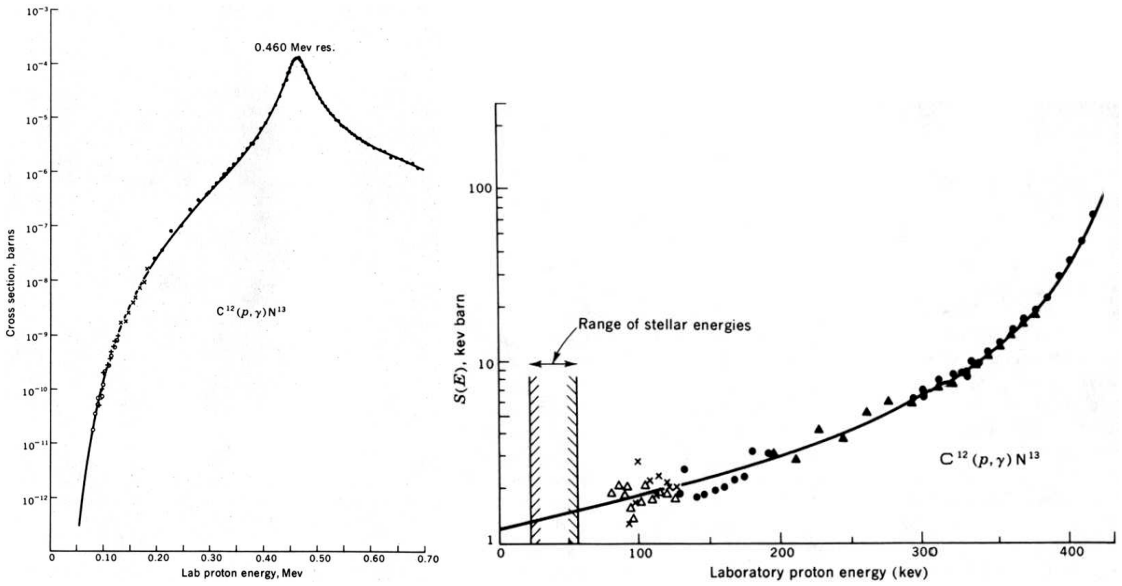

Fig. 7: Cross section and S-factor for the $^{12}C(p,\gamma)^{13}N$ reaction [3].

The nuclear cross section (of s-wave interacting particles) was parametrized by Bethe and Gamow based on general principles of quantum mechanics, as:

$$\sigma(E) \quad = \frac{S(E)}{E} \times e^{-2\pi\eta} \tag{8}$$

where η is the Sommerfeld parameter, $\eta = \frac{Z_1 Z_2 e^2}{\hbar v}$. It is immediately clear that 1/E originates from the $\frac{\pi}{k^2}$ that appears in the expression for the cross section in reaction theory, and the exponent accounts for the penetration factor of the two charged particles Z_1 and Z_2.

3.2 Non Resonant Reactions:

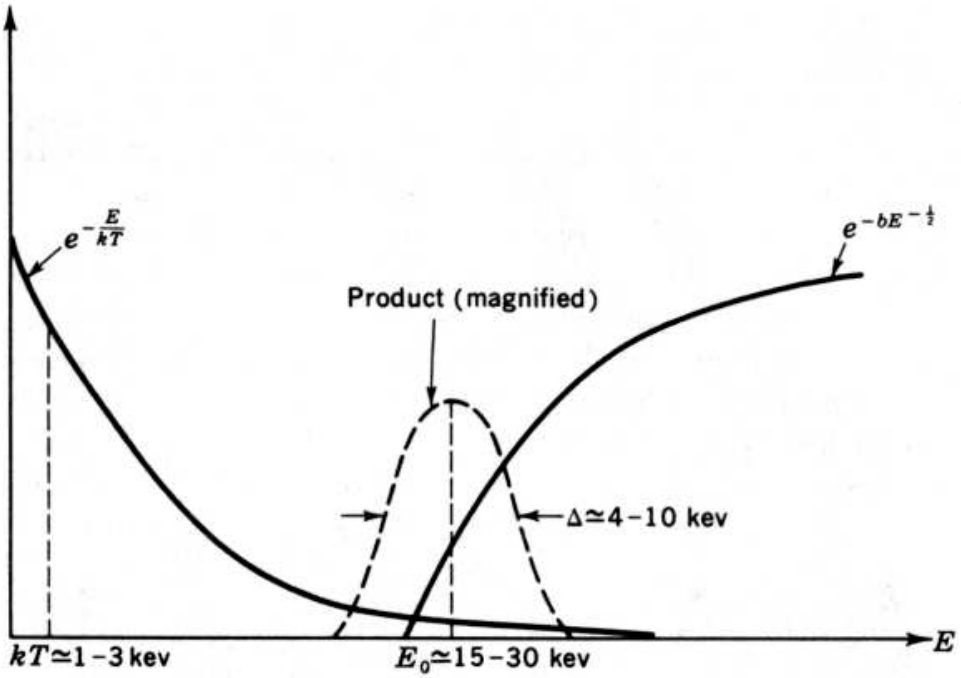

Fig. 8: The Gamow window predicted by equations 10 and 11 [3] for the $^{12}C(p,\gamma)^{13}N$ reaction.

The reaction cross section and S-factor for the $^{12}C(p,\gamma)^{13}N$ are shown in Fig. 7. The region of interest for stellar environment around 30 keV, (the CNO cycle, see below) is indicated in the Figure, and it lies just beyond the region where experiments are still possible (i.e. cross section of 20 pbarns). It is clear that one needs to extrapolate to the energy region of stellar conditions and the extrapolation of the S-factor allows for additional confidence, since the S-factor varies more slowly. Inserting equation 8 to 7, we find:

$$\lambda = <\sigma v> \quad = (\tfrac{8}{\mu\pi})^{1/2} \times \tfrac{1}{(kT)^{3/2}} \int S(E) \times e^{-[\frac{E}{kT}+\frac{b}{E^{1/2}}]}\, dE \qquad (9)$$

where we abbreviated $b = \pi Z_1 Z_2 \alpha (2\mu c^2)^{1/2}$, and $\alpha = \frac{e^2}{\hbar c}$. And for a constant S-factor (S_0) we have:

$$= (\tfrac{8}{\mu\pi})^{1/2} \times \tfrac{S_0}{(kT)^{3/2}} \int e^{-[\frac{E}{kT}+\frac{b}{E^{1/2}}]}\, dE \qquad (10)$$

In this case one finds that the convolution of the Maxwellian and cross section leads to a window of most efficient energy (E_0) for burning, the Gamow window, as shown in Fig. 8.

$$E_0 = (\frac{bkT}{2})^{3/2}$$

$$= 1.22(Z_1^2 Z_2^2 \times A \times T_6^2)^{1/3}\ keV \qquad (11)$$

where T_6 is the temperature in million degrees Kelvin, and $A = \frac{A1A2}{(A1+A2)}$. For example helium burning in Red Giants occurs at 200 MK ($T_6 = 200$), hence the reaction $^{12}C(\alpha,\gamma)^{16}O$ needs to be measured at energies of approximately 315 keV where helium burning is most effective. As we shall see below this turned out to be a formidable task.

3.3 Resonant Reactions:

In many cases the relevant reaction rates are governed by a resonant nuclear state. Such states are either low lying and with narrow width, or higher lying but acquire large width ($\Gamma > 0.1E_r$), and can contribute significantly to the reaction rate at low energies. For narrow states the contribution to the thermonuclear rate arises from the tail (at higher temperatures) of the Boltzmann distribution and for the broad state the thermonuclear rate arises from the tail (at lower energies) of the resonant state.

The cross section for an interaction of particles a + b, of spins J_1 and J_2, in a relative angular momentum state ℓ via an isolated low lying (at E_r close to threshold) nuclear state, is given by the Breit-Wigner formula:

$$\sigma_{r,\ell}(a,b) = \frac{2\ell+1}{(2J_1+1)(2J_2+1)} \times \frac{\pi}{k^2} \times \frac{\Gamma_a\Gamma_b}{(E-E_r)^2+(\frac{\Gamma}{2})^2} \qquad (12)$$

with Γ_i the partial widths and the total width $\Gamma = \sum_i \Gamma_i$. The partial widths are given by, $\Gamma_i = 2P_\ell\gamma_i^2$, where γ_i^2 is the reduced width and P_ℓ the penetrability factor, e.g. the Coulomb penetrability:

$$P_\ell = \frac{kR}{G_\ell^2+F_\ell^2}$$

Note that since the pentrability factor is a property of the exterior region (of the nuclear potential), the results are independent of the choice of the penetration factor (e.g. WKB penetration Vs. Coulomb penetration factor), but strongly depends on the choice for nuclear radii. One defines the statistical factor $\omega = \frac{(2J+1)}{(2J_1+1)(2J_2+1)}$. Note that for most reaction rates the total width are exhausted by one particle width (with other particle widths being energy forbidden), and the radiation width is much

smaller. However the radiation width is the one that allows the resonant state to de-excite to the ground state and hence form the element of interest, as we illustrate in Fig. 9. Cross sections of astrophysical interest are small for energies near the resonant energy due to the smallness of the radiation width ($\frac{\Gamma_\gamma}{\Gamma} \approx 10^{-5} - 10^{-7}$), and at energies below resonance they are hindered by the penetrability. It is immediately clear that the cross section is most directly affected by the energy of the nuclear state, the lower the resonant energy the larger the cross section. And the width of the state is second in this hierarchy.

For a broad state we can write the S-factor:

$$S(E) = \frac{\pi\hbar^2}{2\mu}\,\omega\,\frac{\Gamma_1\Gamma_2}{(E-E_r)+\Gamma^2/2}e^{2\pi\eta} \qquad (13)$$

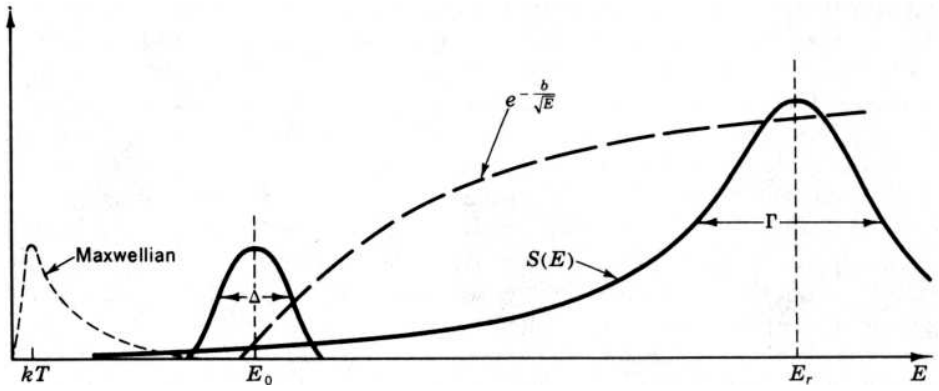

Fig. 9: Nuclear reaction governed by a (broad) nuclear state [3].

For computational purpose it is useful to remember that $\hbar c = 197.33$ MeV fm and $\alpha = 1/137.03$, hence $e^2 = 1.44$ MeV fm. In many cases the evaluation of thermonuclear reaction rates is reduced to accurate measurements of the partial widths that appear in equation 12 [35]. When measurements are not possible one attempts to calculate the S-factor with the use of standard nuclear models such as sum-rules [26, 36], and the thermonuclear cross section could be calculated using equations 9 or 10. We see here that the investigation of the properties of nuclear states, i.e. Nuclear Structure Studies, are directly linked to Nuclear Astrophysics.

For a narrow state we drive the thermonuclear rate:

$$\lambda_i = \hbar^2\left(\frac{2\pi}{\mu kT}\right)^{3/2}\omega_i\frac{\Gamma_1\Gamma_2}{\Gamma}e^{-\frac{E_r}{kT}} \qquad (14)$$

And it is immediately clear that the reaction is possible due to the tail of the Boltzmann factor, or the last term on the right hand side of equation 14.

In the following we shall use concepts that we developed in the above discussion of reaction theory to discuss particular processes in stars.

3.3.1 The PP Chain(s):

Stars in the main sequence like our sun, spend most of their energy generating lifetime burning hydrogen. The burning of hydrogen occurs in several chains known as the PP chains [3, 6], as we list below:

$$\begin{array}{l} {}^1H \ + \ {}^1H \rightarrow \ {}^2D \ + \ e^+ \ + \ \nu_e \\ {}^2D \ + \ {}^1H \rightarrow \ {}^3He \ + \ \gamma \\ {}^3He \ + \ {}^3He \rightarrow \ {}^4He \ + \ 2 \ {}^1H \end{array} \qquad \underline{\text{PPI}}$$

$$\begin{array}{l} {}^3He \ + \ {}^4He \rightarrow \ {}^7Be \ + \ \gamma \\ {}^7Be \ + \ e^- \rightarrow \ {}^7Li \ + \ \nu_e \\ {}^7Li \ + \ {}^1H \rightarrow \ 2 \ {}^4He \end{array} \qquad \underline{\text{PPII}}$$

$$\begin{array}{l} {}^7Be \ + \ {}^1H \rightarrow \ {}^8B + \gamma \\ {}^8B \ \rightarrow \ {}^8Be \ + \ e^+ \ + \ \nu_e \\ {}^8Be \ \rightarrow \ 2 \ {}^4He \end{array} \qquad \underline{\text{PPIII}}$$

The PPI chain is the main source of energy in the sun. It amounts to the fusion of 4 protons to a helium nucleus with the release of approximately 25 MeV energy, and 95% of the photon luminosity is produced within 0.36 $M_\odot$ and $R \ < \ 0.21 \ R_\odot$. The majority of the energy is released in a form of heat (kinetic energy of alpha-particles) and radiation (gamma rays), and some energy (2.3%) is released in the form of solar neutrino's. The reaction rate is dictated by the weak interaction process, the first process in the PPI chain, with a calculated S-factor $S(0) \ = \ 3.78 \pm 0.15 \times 10^{-22}$ keV-barn and linear term coefficient $\frac{dS}{dE} \ = \ 4.2 \times 10^{-24}$ barn. Inserting this S-factor and T = 15 MK, with the solar density of $\rho \ = \ 150 \ g/cm^3$ and $X_{He} \ = \ X_H \ = \ 0.5$, in equation 9 we derive a reaction time, $\lambda^{-1} \ = \ 10 \ GY$, i.e. the expected lifetime of the sun. Using available luminosities (i.e. available beams and targets) we expect in the laboratory at energies of astrophysical interest, an approximate rate of one p + p interaction per year, which is clearly non measurable. However, this rate is considered to be reliable (within ±1%) as it is extracted from known weak interaction rates such as the neutron lifetime. We also note that the PPI neutrino luminosity (see above) is directly calculable from the total luminosity of the sun and thus the PPI neutrino flux is considered to be estimated with great certainty.

The burning of hydrogen release a large flux of neutrino's and with the knowledge of the various branching ratio's and reaction rates we derive [6, 37] for the standard solar model the neutrino flux as shown in Fig. 10.

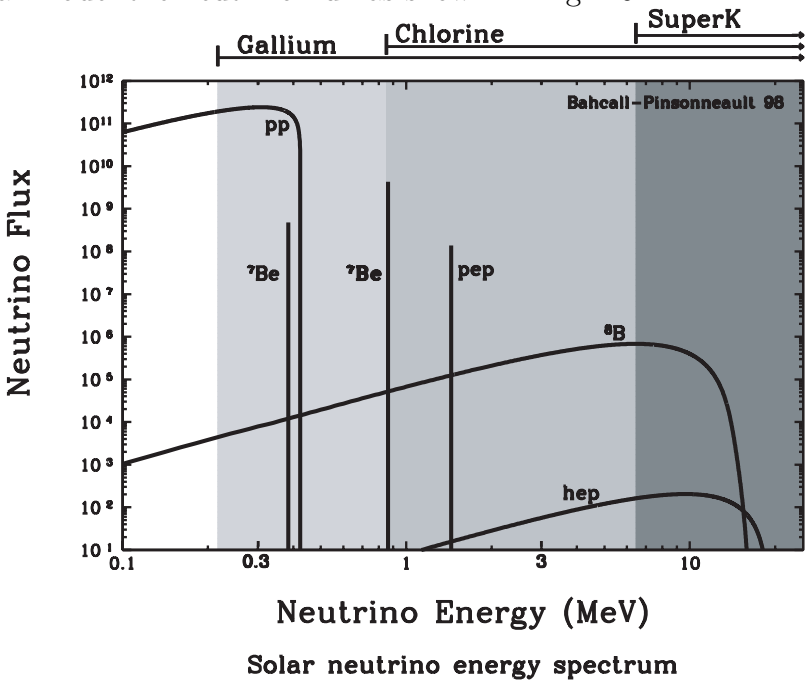

Fig. 10: Predicted Solar neutrinos fluxes [6].

3.3.2 The Solar Neutrino Problem:

Attempts to measure solar neutrino's were carried out over the last two decades [6]. The detection of solar neutrinos is expressed in terms of the SNU, the Solar Neutrino Unit, which is the product of the calculated characteristic solar neutrino flux (in units of $cm^{-2}sec^{-1}$) times the theoretical cross section for neutrino interaction in the detector (in units of cm^2). Hence the SNU is in units of rate, events per target atom, per second, and is chosen for convenience equal to $10^{-36}\ sec^{-1}$. For a detector with 10^{31} atoms, one SNU yields one interaction per day. This counting rate is characteristic of solar neutrino detectors.

The first neutrino detector was constructed over three decades ago in the Homestake mine, by Raymond Davis Jr. [6] and it includes 10^5 gallons of the cleaning agent carbon tetra chloride. In this detector neutrino's with energies above 800 keV (threshold) yield the reaction:

$$\nu_e \ + \ ^{37}Cl \ \rightarrow \ e^- \ + \ ^{37}Ar \qquad (15)$$

and the nobel gas argon is collected by bubbling helium through the tank and collecting it in chemical adsorbers. The decay products of the activity of ^{37}Ar are counted in a proportional counter in a low background environment. For this chlorine detector one predicts using Bahcall-Uhlrich Standard Solar Model and Bahcall-Pinsonneault SSM [37, 38] $7.9 \pm 2.6\ SNU's$. The observed rate of the Chlorine detector is averaged over the last three decades of counting to yield the quoted rate of: $2.2 \pm 0.2\ SNU$, or for example $28\% \pm 3\%$ of the rate predicted by Bahcall and Uhlrich [37]. The B-U model was later improved by Bahcall and Pinsonneault [38] and predict yet higher ^8B neutrino flux. As we discuss below other solar models that use different nuclear inputs (see below the S_{17} problem) predict a smaller neutrino fluxes [39, 40, 41].

The Kamiokande proton decay detector (Kamiokande I) was outfitted for a solar neutrino detector (Kamiokande II) and was used since January 1987. It detects the Cerenkov radiation of electrons elastically scattered by the neutrino's and it had at first a threshold of approximately 9.5, which was later improved to 7.5 MeV. This detector observed after approximately 1000 days of counting $46\% \pm 5\%(stat) \pm 6\%(syst)$ of Bahcall's predicted flux [42]. Kamiokande III which consists of improved detection systems with larger efficiency for light collection using extensive mirrors and water considerably cleaner with less Rn contaminant(s) and hence smaller threshold (7 MeV), in operation since 1991 [43], reported $56\% \pm 6\%(stat) \pm 6\%(syst)$ of Bahcall's predicted flux. The average of six years of counting with the Kamioka detector amounts to $50\% \pm 4\%(stat) \pm 6(syst)$ of the B-U Standard Solar Model [43] and 66% of the SSM of Turck-Chieze and Lopez [40, 41]. For over two years a new SuperKamiokande detector came to operation and is taking data with threshold as low as 5 MeV and it quoted the rate [44] of $35.8\% +0.9-0.8\%(stat) +1.4-1.0\%(syst)$ of the Bahcall and Pinsonneault [38] predicted rate.

More recently results from gallium detectors were reported. These detectors have a very low threshold, of 233 keV, and hence detect the neutrinos of the PPI chain, that extends to approximately 400 keV. In fact the detection of the PPI neutrino's constitute the first direct evidence that the sun burns hydrogen as its primary source of energy. The (updated) SAGE collaboration reported [45] 70 ± 20 SNU's and the GALLEX collaboration [46] (updated) rate is: $79 \pm 10(stat) \pm 7(syst)$, compared to the expected rate of $132 +20 -17\ SNU's$. The PPI neutrino's contribute most of the predicted rate for Ga detectors (approximately 55%) and for PPI neutrino's all theoretical predictions are within a reasonable agreement of each other, and for example Turch-Chieze predicts 125 ± 7 SNU expected Ga detection rate.

The Sudbury Neutrino Observatory (SNO) detector [47, 48] became operational in 1999 [49]. This detector uses 1000 tons of heavy water and is expected to have

a much improved performance, as well as detect a variety of additional neutrino processes such as neutral current interactions, and would also serve as a neutrino spectrometer.

The most popular theoretical interpretation of the hindrance of the solar neutrino flux, by approximately a factor of 2, is the neutrino flavor oscillation induced by a density dependent resonance effect, known as the MSW effect [50, 51]. We however note that in order to reconcile all the currently available data in one theoretical frame, one requires additional energy dependence of the resonance process with 1 MeV neutrinos maximaly oscilating.

3.3.3 The CNO cycle:

In 1939 in a seminal paper delivered in a meeting at Washington DC, Hans Bethe proposed that stars slightly more massive then the sun ($M > 2M_{\odot}$, but with temperatures smaller then 100 MK, may generate their energy more efficiently by burning hydrogen with the help of carbon (i.e. carbon is acting as a catalyst), now known as the CNO cycle. The main branch of the CNO cycle:

$$^{12}C(p,\gamma)^{13}N(\beta^{+})^{13}C(P,\gamma)^{14}N(p,\gamma)^{15}O(\beta^{+})^{15}N(p,\alpha)^{12}C \qquad (16)$$

$$^{12}C(p,\gamma)^{13}N(p,\gamma)^{14}O(\beta^{+})^{14}N(p,\gamma)^{15}O(\beta^{+})^{15}N(p,\alpha)^{12}C \qquad (16a)$$

We note that indeed in the CNO process, equation 16, like in the PP chain, four protons were used to produce a helium nucleus, with the production of fusion energy and the emission of electron neutrino's. In addition the star will now have carbon and nitrogen isotopes at various concentrations due to this cycle. For stars of core temperature larger then 17 MK [7] the CNO cycle provides a more efficient energy source and indeed these stars generate a large fraction of their energy through the CNO cycle as shown in Fig. 11.

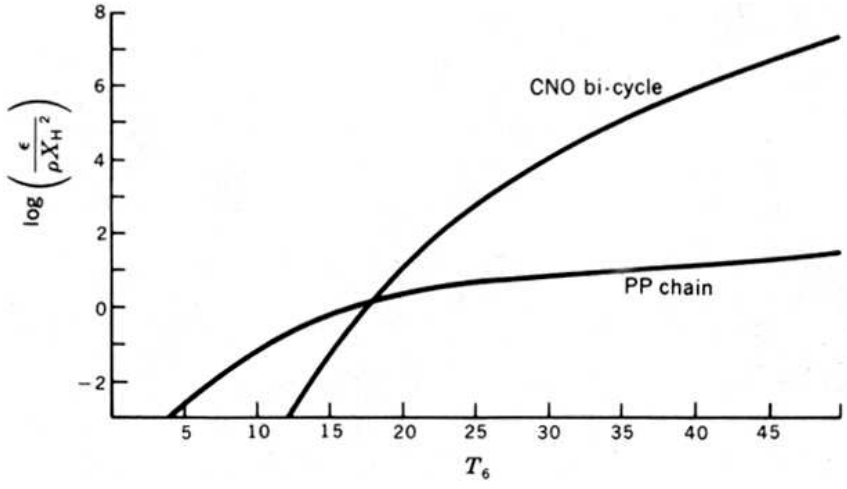

Fig. 11: The CNO - PP transition [3].

3.3.4 The hot CNO cycle:

The beta decay lifetime of ^{13}N is 863 sec and of ^{15}O is 176.3 sec. The lifetime of ^{13}N is slow enough to allow for a different branch of the CNO cycle to develope, see equ. 16a. Clearly if the temperatures and densities rises, such as in explosive hydrogen stellar environments, it should be possible to reach a point where the $^{13}N(p,\gamma)^{14}O$ reaction rate is fast enough that it could favorably compete with the slow beta decay of ^{13}N, leading to the hot-CNO cycle, equ. 16a. This rate is given by equation 6, $\frac{1}{<\sigma v>N_{13}} < 863$ sec, and the conditions are related to the reaction cross section, density and temperatures. One then clearly needs to know the cross section for the reaction $^{13}N(p,\gamma)^{14}O$ at low energies, in order to determine the stellar conditions (density and temperature) where stars may break into the hot CNO cycle. This reaction is governed by the 1^- state at 5.17 MeV in ^{14}O, as shown in Fig. 12.

The hot CNO cycle is found in hydrogen rich environments, at large temperatures and densities, usually involving a binary star system(s) such as Novae etc., hence further capture of protons and alpha-particles on elements from the hot CNO cycle may allow for break out of the hot CNO cycle and into the rp process [52]. In this case the production of ^{19}Ne via the $^{15}O(\alpha,\gamma)^{19}Ne$ reaction, and various related branches of the hot-CNO cycle, play a major role. These processes may in fact produce yet heavier elements, such as ^{22}Ne and elements as heavy as mass 60 nuclei, however we will not cover in this lecture notes these processes.

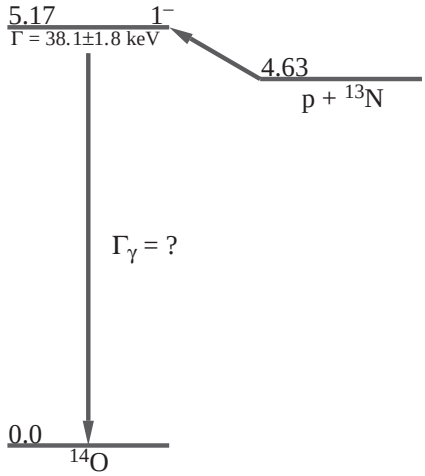

Fig. 12: Nuclear states in ^{14}O relevant for the hot-CNO cycle.

3.3.5 Nucleosynthesis in Massive Stars:

As stars consume their hydrogen fuel in the core, now composed mainly of helium, it contracts, raising its temperature and density. For example, in 25 solar masses stars the hydrogen burning last for 7 Million years. At temperatures of the order of 200

MK [4], the burning of helium sets in. The first reaction to occur is the $\alpha + \alpha \rightarrow {}^{8}Be$ due to the short lifetime of ${}^{8}Be$ this reaction yield a small concentration of ${}^{8}Be$ nuclei in the star. However, this reaction is very crucial as a stepping stone for the next reaction that is loosely described as the three alpha-capture process:

$$ {}^{8}Be(\alpha,\gamma)^{12}C \tag{17}$$

The formation of small concentration of ${}^{8}Be$, allows for a larger phase space for the triple alpha-capture reaction to occur. This reaction was originally proposed by Fred Hoyle, as a solution for bridging the gap over the mass 5 and 8, where no stable elements exist, and therefore the production of heavier elements. In fact the triple alpha capture reaction is governed by the excited 0^{+} state in ${}^{12}C$ at 7.654 MeV, as shown in Fig. 13. This state was predicted by Fred Hoyle prior to its discovery (by Fred Hoyle and others) at the Kellog radiation lab [30]. One loosely refers to this 0^{+} state as the reason for our existence, since without this state the universe will have a lot less carbon and indeed a lot less heavy elements, needed for life. Extensive studies of properties of this state by nuclear spectroscopist allow us to determine the triple alpha-capture rate using equation 14. The triple alpha process is in fact accurately known to better then 10%. A possible alternative to the formation of ${}^{12}C$ was suggested via the hot pp cycle [53]: the reaction chain ${}^{7}Be(\alpha,\gamma)^{11}C(p,\gamma)^{12}N(\beta^{-})^{12}C$.

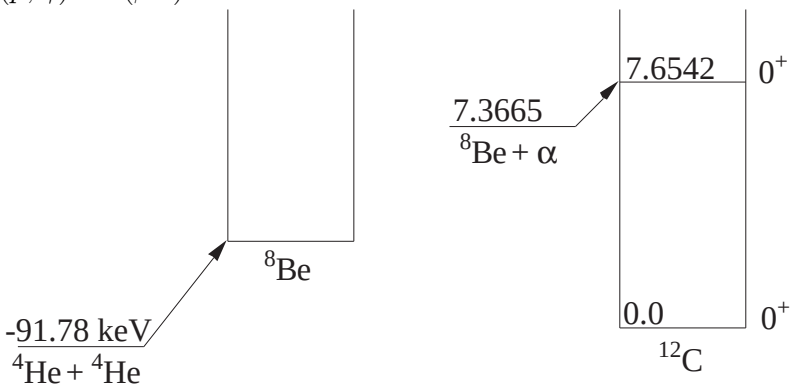

Fig. 13: Nuclear levels in ${}^{12}C$ and ${}^{8}Be$, relevant for the triple alpha-particle capture reaction.

At the same temperature range (200 MK), the produced ${}^{12}C$ nuclei can undergo subsequent alpha-particle capture to form ${}^{16}O$:

$$ {}^{12}C(\alpha,\gamma)^{16}O \tag{18}$$

Unlike the triple alpha-capture reaction this reaction occurs in the continuum, as shown in Fig. 14. This reaction is governed by the quantum mechanical interference of the tail of the bound 1^- state at 7.12 MeV (the ghost state) and the tail of the quasi-bound 1^- state at 9.63 MeV, in ^{16}O. As we shall see in section 4 of this lecture notes, these effects eluded measurements of the S-factor of $^{12}C(\alpha,\gamma)^{16}O$ reaction for the last two decades, in spite of repeated attempts. More recently great hopes were introduced for solving this problem [54] via beta-delayed alpha-particle emission of ^{16}N [55, 56, 62], but this hopes appear to have faded away [63, 64, 65], as we discuss below. Helium burning lasts for approximately 500,000 years in a 25 solar mass star [4], and occurs at temperatures of approximately 200 MK. As we shall see below the outcome of helium burning (i.e. the ratio between carbon and Oxygen) is very crucial for determining the final fate of a massive star prior to its supernova collapse.

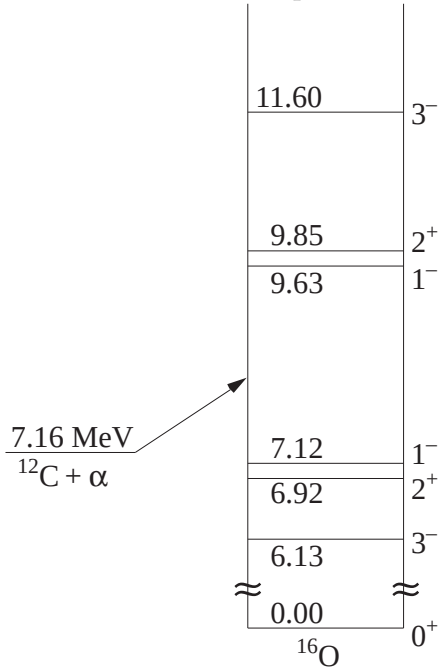

Fig. 14: Nuclear levels in ^{16}O relevant for helium burning.

Stars of masses smaller then approximately 8 solar masses will complete their energy generating life cycle at the helium burning cycle. They will be composed mainly of carbon and oxygen and contract to a dwarf lying forever on the left bottom corner of the H-R diagram. More massive stars at the end of helium burning, commence carbon burning at a temperature of approximately 600-900 MK. Carbon burning lasts for 600 years in 25 solar masses stars [4]. The main reaction process in carbon burning is the $^{12}C(^{12}C,\alpha)^{20}Ne$ reaction, but elements such as ^{23}Na, and some ^{24}Mg are also produced. At temperatures of approximately 1.5 BK (or approximately 150 keV) the tail of the Boltzmann distribution allows for the photo-

disintegration of ^{20}Ne, with an alpha-particle threshold as low as 4.73 MeV. This reaction $^{20}Ne(\gamma,\alpha)^{16}O$ serves as a source of alpha-particle which are then captured on ^{20}Ne to form ^{24}Mg and ^{28}Si. The neon burning cycle lasts for 1 year in a 25 solar masses stars. These alpha-particles could also react with ^{22}Ne, as suggested by Icko Iben [66], to yield neutron flux via the $^{22}Ne(\alpha,n)^{25}Mg$ reaction and give rise to the slow capture of neutrons and the production of the heavy elements via the s-process. At this point the core is rich with oxygen, and it contracts further and the burning of oxygen commence at a temperature of 2 BK, mainly via the reaction $^{16}O(^{16}O,\alpha)^{28}Si$, with the additional production of elements of sulfur and potassium. The oxygen burning period lasts for approximately 6 months in a 25 solar masses star [67]. At temperatures of approximately 3 BK a very brief (one day or so) cycle of the burning of silicon commence. In this burning period elements in the iron group are produced. These elements can not be further burned as they are the most bound (with binding energy per nucleon of the order of 8 MeV), and they represent the ashes of the stellar fire. The star now resemble the onion like structure shown in Fig. 15.

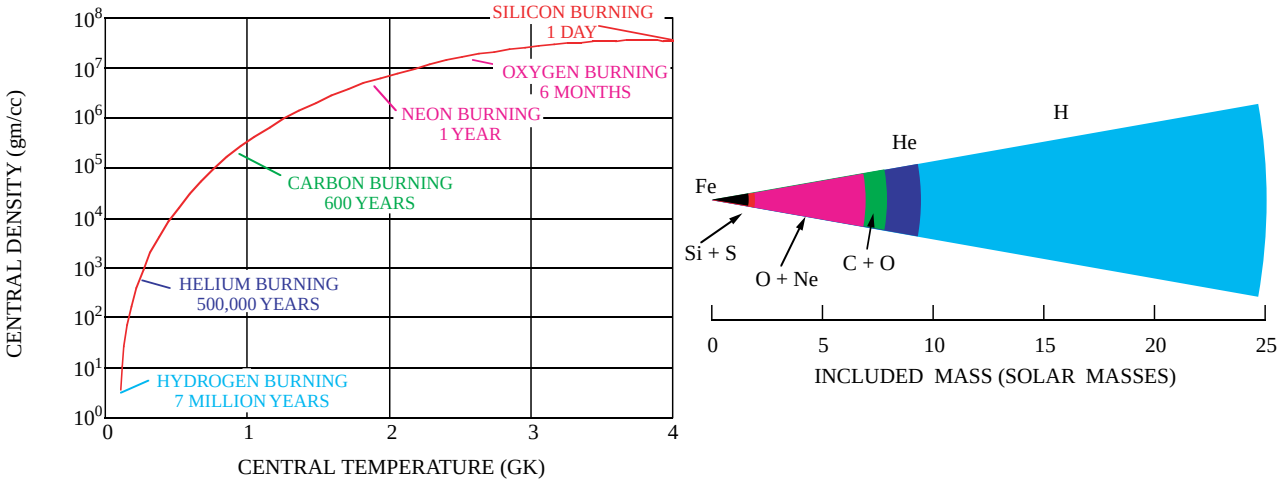

Fig. 15: Burning stages and onion-like structure of a $25M_{\odot}$ star prior to its supernova explosion [4, 67].

As the inactive iron core aggregates mass it reaches the Chandrasekar limit (close to 1.4 solar mass) and it collapses under its own gravitational pressure, leading to the most spectacular event of a supernova. During a supernova the electrons are energetic enough to undergo electron capture by the nuclei and all protons are transposed to neutrons, releasing the gravitational binding energy (of the order of $\frac{3}{5}\frac{GM^2}{R} \approx 3 \times 10^{53}$ ergs) mostly in the form of neutrino's of approximately 10 MeV (and temperature of approximately 100 GK). As the core is now composed of compressed nuclear matter (several times denser then nuclei), it is black to neutrino's (i.e. absorbs the neutrino's) and a neutrino bubble is formed for approximately 10 sec, creating an outward push of the remnants of the star. This outward push is believed

by some to create the explosion of a type II supernova. During this explosion many processes occur, including the rapid neutron capture (r process) that forms the heavier elements of total mass of approximately $M \approx 2\% M_{\odot}$.

The supernova explosion ejects into the inter-stellar medium its ashes from which at a later time "solar systems" are formed. Indeed the death of one star yields the birth of another. At the center of the explosion we find a remnant neutron star or a black hole, depending on the outcome of helium burning.

One of the early records of supernova was provided by Chinese astronomers from July 4th 1054 AD [4]. That explosion left behind a cloud known as the Crab Nebula. Additional observation were made by Ticho Braha and later by his student Kepler. These include a supernova explosion on October 8, 1604 AD in the constellation Ophiuchus, shown in Fig. 16 [68, 69] and one in 1667 AD in the constellation Cassiopeia A. Some speculate that the star of Beth-Lechem may correspond to a supernova explosion that occurred in the year 3 AD. More recent explosions, supernova 1987A and 1993J allowed for a more detailed examination of the nucleosynthesis as well as the observation(s) of neutrino's from such explosions.

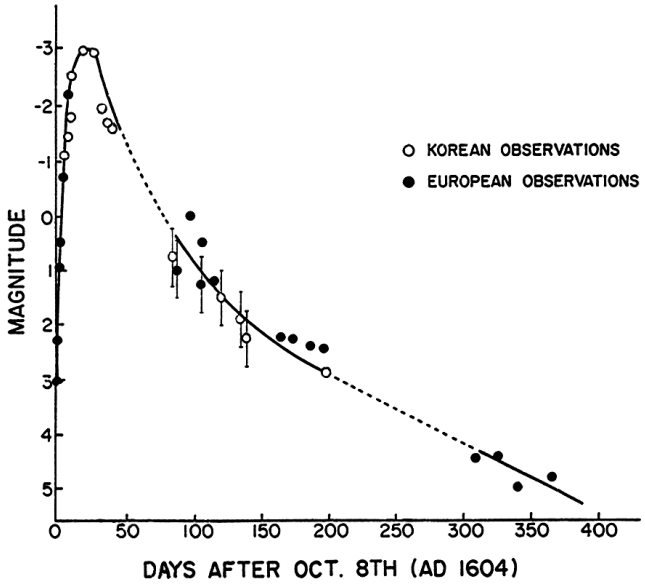

그림 3

Fig. 16: Light curves obtained from western and eastern historical records, indicating a type I supernova [68, 69].

It is clear from Fig. 15, that if in the process of helium burning mostly oxygen is formed, the star will be able to take a shorter route to the supernova explosion. In fact if the carbon to oxygen ratio at the end of helium burning in a 25 solar masses star, is smaller then approximately 15% [70], the star will skip the carbon and neon

burning and directly proceed to the oxygen burning. In Fig. 17 we show the results of the neon burning as a function of the S-factor for the $^{12}C(\alpha,\gamma)^{16}O$ reaction [70], and clearly for a cross section of the $^{12}C(\alpha,\gamma)^{16}O$ reaction that is twice the accepted value [31, 32] (but not 1.7 the accepted value), a 25 solar masses star will not produce ^{20}Ne, and the carbon burning is essentially turned off. This indeed will change the thermodynamics and structure of the core of the progenitor star and in fact such an oxygen rich star is more likely to collapse into a black hole [70] while carbon rich progenitor stars is more likely to leave behind a neutron star. Hence one needs to know the carbon to oxygen ratio at the end of helium burning (with an accuracy of the order of 15%) to understand the fate of a dying star and the heavy elements it produces.

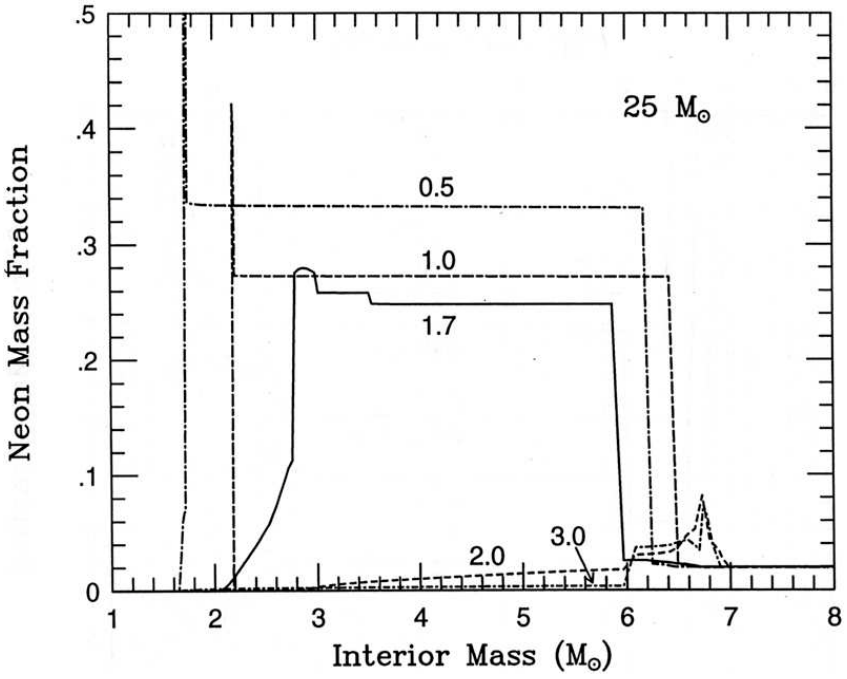

Fig. 17: Neon Formation; the turning off of carbon burning (at twice the [31] accepted value for the $^{12}C(\alpha,\gamma)^{16}O$ reaction), is evident by a small production of neon [70].

Since the triple alpha-particle capture reaction: $^{8}Be(\alpha,\gamma)^{12}C$ is very well understood, see above, one must measure the cross section of the $^{12}C(\alpha,\gamma)^{16}O$ reaction with high accuracy of the order of 15% or better. Unfortunately as we discuss in the next chapter this task was not possible over the last two decades using conventional techniques and initial hopes spured by the measurement of the beta-delayed alpha-particle emission of ^{16}N [55, 56, 62], did not materialize either [63, 64, 65].

4 CENTRAL PROBLEMS IN NUCLEAR ASTROPHYSICS

In this chapter we review some of the central problems of nuclear astrophysics. We review the difficulties encountered and in some cases suggest that radioactive beams could be used to solve these critical problems of nuclear astrophysics.

4.1 The ^8B solar Neutrino's and the $^7Be(p,\gamma)^8B$ Reaction:

The predicted PPI solar neutrino flux is NOT sensitive to the details of the weak interaction nuclear process and only depends on knowledge of the luminosity of the sun, 1.37 kW/m^2 at 1 AU, and $L_\odot = 3.86 \times 10^{33}\ erg\ sec^{-1}$. This conclusion is due to the fact that the kinematics of hydrogen burning in the PPI chain requires that approximately 2.5% of the solar luminosity is radiated with neutrinos. The flux of the ^8B solar neutrino's, composing 75% of those detected by Ray Davis' chlorine detector, and 100% of the Kamiokande detector and also the SNO detector, on the other hand is very sensitive to the details of the nuclear inputs and in particular to the $^7Be(p,\gamma)^8B$ reaction, as well as the exact solar model including opacities and central temperatures.

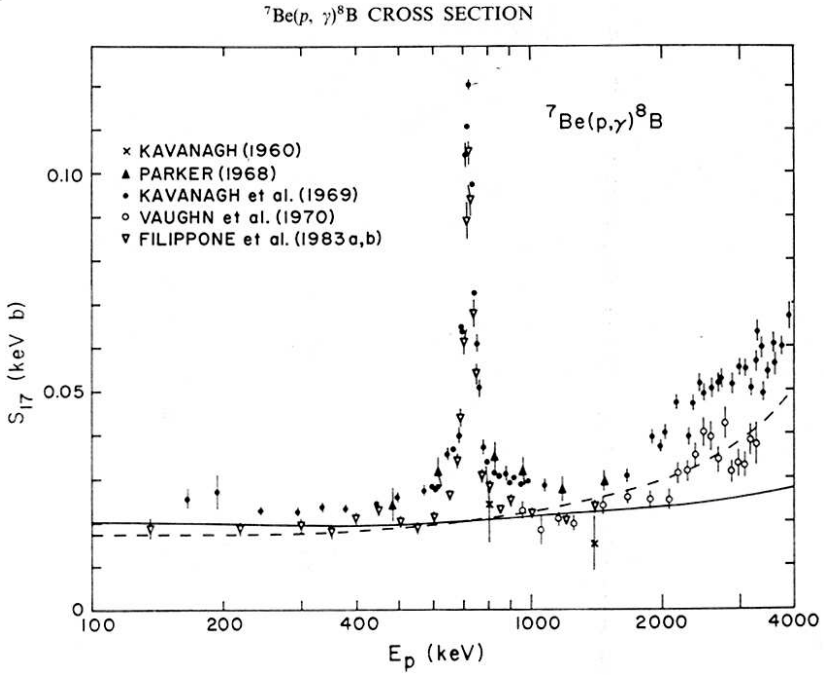

Fig. 18: The extrapolated S_{17} factor of Barker and Spear, who first suggested a low value of $S_{17}(0)$ of 17 eV-b [71].

The accepted value of the S-factor used by Bahcall and Uhlrich [37] for the $^7Be(p,\gamma)^8B$ reaction at zero energy is, $S_{17} = 24.3$ eV-barn. The more recent

value adopted by Bahcall and Pinsonneault [38] is 22.4 eV-b. Turck-Chieze adopted the value measured by Filippone of 20.9 eV-b [39]. This small value is one of the most significant differences between her SSM and Bahcall's SSM. The value of S_{17} was studied in details by Barker and Spear [71] and Jonson, Kolbe, Koonin and Langanke [72]. Barker and Spear point out to problems in the value of normalization used for the $^7Be(p,\gamma)^8B$ studies, i.e. the $^7Li(d,p)^8Li$ reaction. They discuss the evolution of the value of the $^7Li(d,p)^8Li$ reaction cross section measured on the 770 keV resonance, as well as other factors and suggest the very low value of $S_{17} = 17$ eV-b, or approximately a 30% reduction in S_{17} as compared to the value adopted by Bahcall and Uhlrich, as shown in Fig. 18. This would imply a reduction of 30% in the expected ^8B solar neutrino flux, indeed a large decrease. Johnson et al. point out to some discrepancies between data obtained by Filippone et al. [73] and the unpublished data of Kavanagh et al. [74]. Johnson et al. [72] adopt the value of $S_{17} = 22.4$ eV-b, as adopted by Bahcall and Pinsonneault but 8% below the value accepted by Bahcall and Uhlrich, as shown in Fig. 19.

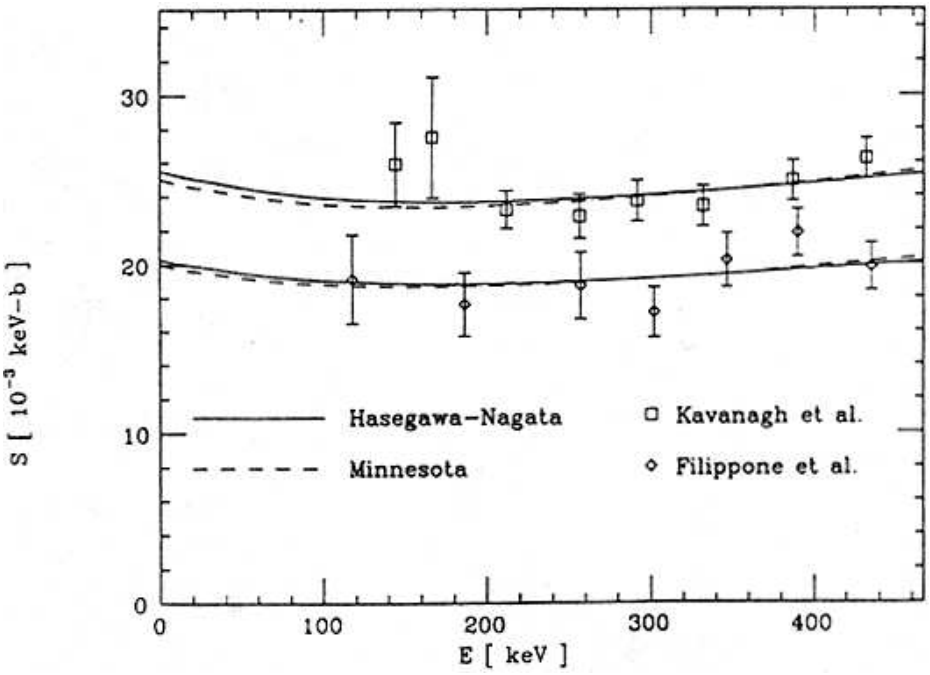

Fig. 19: Comparison of the measurement of Filippone [73] and Kavanagh [74]. And the S_{17} factor extracted by Johnson et al [72].

In Fig. 20 we show the ratio of the cross sections measured by Filippone et al. [73], Kavanagh et al. [74], Parker [75], and Vaughn et al. [76]. The data of Parker and Kavanagh et al. are in agreement with each other, as are the data of Filippone et al. and Vaughn et al. The two data sets are also in good agreement on the energy dependence of the two cross sections. However as shown in Fig. 20 the two data sets

are in disagreement by approximately 35% on the absolute value of the cross section.

In a recent review of Solar fusion cross section [77] in a workshop in the INT at Seattle the cross section of the $^7Li(d,p)^8Li$ and S_{17} were reviewed with a re-eavluation of $\sigma_{dp} = 147 \pm 11$ [77, 78, 79] and $S_{17}(0) = 19 + 4 - 2$ eV-b. More recent direct measurements with a ^7Be radioactive [80, 81] agree with the lower value adopted by the Seattle workshop [77]. A new ^7Be radioactive target produced at TRIUMF [82] allows for yet another mesuement with ^7Be radioactive target, and in the next chapter we discuss the most important experiment with accelerated ^7Be beams.

The importance of the $^7Be(p,\gamma)^8B$ reaction for the evaluation of the ^8B solar neutrino flux calls for a continued interest and additional accurate measurements of the $^7Be(p,\gamma)^8B$ reaction, and in particular measurements that can distinguish between the two absolute values of the cross sections, see Fig. 20, are very much needed. In the next chapter we discuss an interesting new approach with a measure of success success, at attacking this problem with ^8B radioactive beams and the use of a new technique involving the Coulomb Dissociation (Primakoff) process.

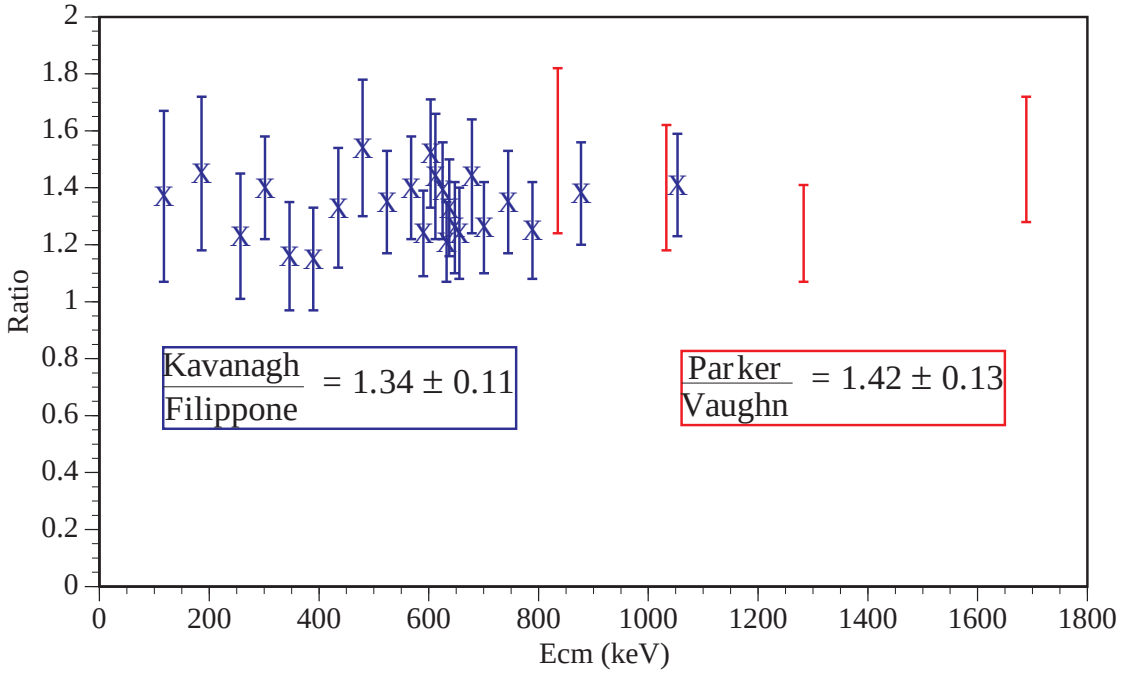

Fig. 20: The ratio of the cross sections for $^7Be(p,\gamma)^8B$ measured by Kavanagh et al. [74] and Parker [75] Vs Filippone et al. [73] and Vaughn et al. [76].

4.2 Extrapolation of S_{17} to Solar Energies

The discrepancy in the measured absolute value of the cross section of the $^7Be(p,\gamma)^8B$ reaction is clearly disturbing and as we show later it is quite possibly best addressed with a ^7Be radioactive beam and a hydrogen target, allowing for a direct measurement

of the beam-target luminosity. However, additional uncertainty exists in the theoretical extrapolation of the measured cross section to solar energies (approximately 20 keV). A few theoretical studies suggest an extrapolation procedure that is accurate to approximately $\pm 1\%$ [83]. Without discussing these rather strong statements we consider a similar situation that haunted Nuclear Astrophysics a few years back– the S-factor of the $d(d,\gamma)^4He$ reaction. It was assumed that in this case d-waves dominate and no nuclear structure effects should play a role at very low energy, as low as 100 keV. Much in the same way, it is stated today that s-waves dominate the $^7Be(p,\gamma)^8B$ reaction and we do not expect nuclear structure effects to play a role at low energies in the $^7Be(p,\gamma)^8B$ reaction. In Fig. 21 we show Fowler's extrapolated d-wave S-factor that is a mere factor of 32 smaller than measured, due to a small non d-wave component in the d + d interaction [84]. A small nuclear structure effect, namely the d-wave component of the ground state of ^4He, gives rise to a change by a factor of 32 in the predicted astrophysical S-factor. Similarly we may ask whether a small non s-wave component in the low energy interaction of p + ^7Be could alter the extrapolated $S_{17}(0)$ value by more than one percent. A measurement of $S_{17}(0)$ with an accuracy of $\pm 5\%$ mandates that the cross section be measured at low energies, as low as possible, so as to also test the extrapolation procedures [83].

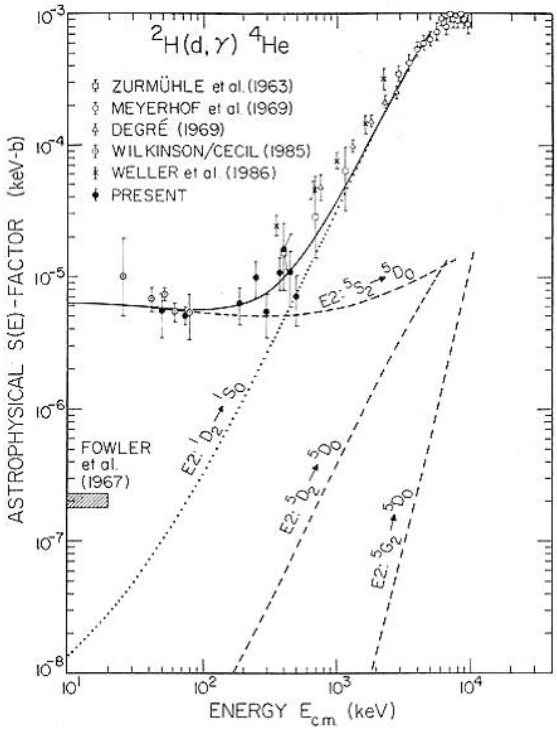

Fig. 21: Extrapolation of d-wave S-factor of the $d(d,\gamma)^4He$ reaction[84]. Note the presence of small non d-wave components that yield a discrepancy from Fowler's extracted S-factor by a factor of 32.

4.3 The Hot CNO cycle and the $^{13}N(p,\gamma)^{14}O$ Reaction:

As we discuss in section 3.3.4, the value of the cross section of the $^{13}N(p,\gamma)^{14}O$ reaction at low energies is governed by the 1^- state at 5.17 MeV in ^{14}O, see Fig. 12. Hence an indirect measurement of the cross section could be carried out by measuring its partial width. The knowledge of the energy of the state [85], its total width [86] and its partial radiative width, or branching ratio for gamma decay [35], should allow for determination of the cross section, see equations 12 and 14. This determination turned out to be a formidable task [87, 88, 89]. In Fig. 22 we show the radiative width extracted in these experiments [35, 87, 88, 89] where it is deduced from a measurement of the branching ratio for the 5.17 MeV gamma decay and the total width of the state [86]. Only the measurement of Fernandez et al. appears useful for this study. As a comment in passing we note that the use of the Energy Weighted Dipole Sum Rule (EWDSR):

$$\begin{aligned} S_1(E1) &= \sum E(1^-) \times B(E1 : 0^+ \ \rightarrow \ 1^-) \\ &= \tfrac{9}{4\pi} \ \tfrac{NZ}{A} \ \tfrac{e^2\hbar}{2m} \end{aligned} \tag{19}$$

yield an upper limit on the radiative width of approximately 5 eV. In this case we assume that the $B(E1: \ 1^- \ \rightarrow \ 0^+)$ does not exhaust more then 1% of the EWDSR. Note that even the largest known B(E1)'s in ^{11}Be and ^{13}N exhaust 0.09% and 0.2% of the EWDSR, and based on our understanding of dipole electromagnetic decays, as first suggested by Gell-Mann and Telegdi [90] and Radicati [91] for self conjugate nuclei, and with advances made by theoretical and experimental studies of B(E1) in nuclei [36], we can estimate that the E1 decay should exhaust less then 1% of the EWDSR, as shown in Fig. 22. The sum rule model then allow us to place an upper limit on the value of the radiative width of the 1^- state. In spite of a concentrated effort and with the exclusion of the Seattle result of Fernandez et al., it is clear that an accurate determination of the partial widths of the 1^- state at 5.17 MeV in ^{14}O is needed. By way of introduction to the next chapter, we show in Fig. 22 the accurate results obtained (in experiments that lasted for only a few days each) with radioactive beams [92, 93, 94].

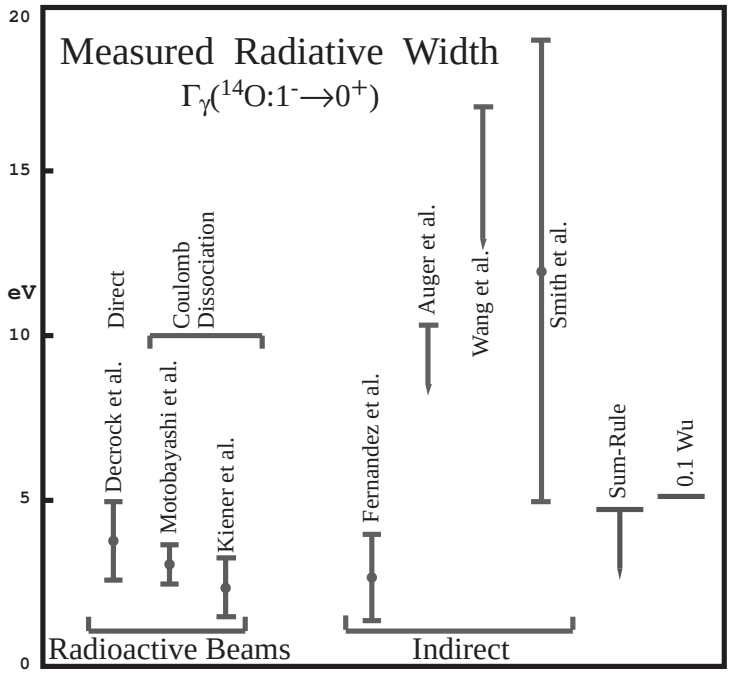

Fig. 22: Measured $\Gamma_\gamma(^{14}O : 1^- \rightarrow 0^+)$ using indirect and direct methods. Most indirect measurements, except for the Seattle one [35], yield results less sensitive then (even) the sum rule. The advent of radioactive beams is clear.

4.4 Helium Burning and the $^{12}C(\alpha,\gamma)^{16}O$ Reaction:

For understanding the process of helium burning and in particular the oxygen to carbon ratio at the end of helium burning we must understand the $^{12}C(\alpha,\gamma)^{16}O$ reaction as in equation 18, at the most effective energy for helium burning of 300 keV, see equation 11. At this energy one may estimate [30] the cross section to be 10^{-8} nbarn, clearly non measurable in laboratory experiments. In fact the cross section could be measured down to approximately 1.2 MeV and one needs to extrapolate down to 300 keV, see Fig. 23. As we discuss below the extrapolation to low energies (300 keV) which in most other cases in nuclear astrophysics could be performed with certain reliability, is made difficult by a few effects.

The cross section at astrophysical energies has contribution from the p and d waves and is dominated by tails of the two bound states of ^{16}O, the 1^- at 7.12 MeV (p-wave) and the 2^+ at 6.92 MeV (d-wave), see Fig. 14. The p-wave contribution arises from a detailed interference of the tail of the bound 1^- state at 7.12 MeV and the broad 1^- state at 6.93 MeV, see Fig. 14. The contribution of the bound 1^- state arises from its virtual alpha-particle width, that could not be reliably measured or calculated. Furthermore, the tails of the quasi-bound and bound 1^- states interfere in the continuum and the phase can not be determined from existing data. Existing data

could be measured only at higher energies and therefore it does not show sensitivity to the above questions. Hence, the cross section of the $^{12}C(\alpha,\gamma)^{16}O$ reaction could not be measured in a reliable way at 300 keV, and the p-wave S-factor at 300 keV, for example, was estimated to be between 0-500 keV barn with a compiled value of $S_{E1} = 60 \, {}^{+60}_{-30}$ keV-b [31, 32] and $S_{E2}(300) = 40 \, {}^{+40}_{-20}$ keV-b. This large uncertainty is contrasted by the need to know the S-factor with 15% accuracy, see chapter 3 and Fig. 17. In Fig. 24 we show the results obtained over two decades for the p- wave S-factor, with the most notable disagreement in the extracted results of the Munster group, that quoted a very large S-factor with a small error bar. We refer the reader to [55, 56, 57, 58, 59, 60, 61] for a complete reference list and review of the subject. The situation is best described as in Fig. 25 where a blind man attempts to find out wether the elephant trunk is up or down by holding its tail. He is clearly performing an experiment with small sensitivity to the question at hand. In the next section we will discuss new idea(s) for measuring this process (in the time reversed fashion with ^{16}O disintegrating to $\alpha + {}^{12}C$). Great hopes for measuring the p-wave S-factor in the beta-delayed alpha-particle emission of ^{16}N [54], turned out to be false and we propose a new experiment, the photodisintegration of ^{16}O, the $^{16}O(\gamma,\alpha)^{12}C$ to be performed at the Duke-HIGS facility.

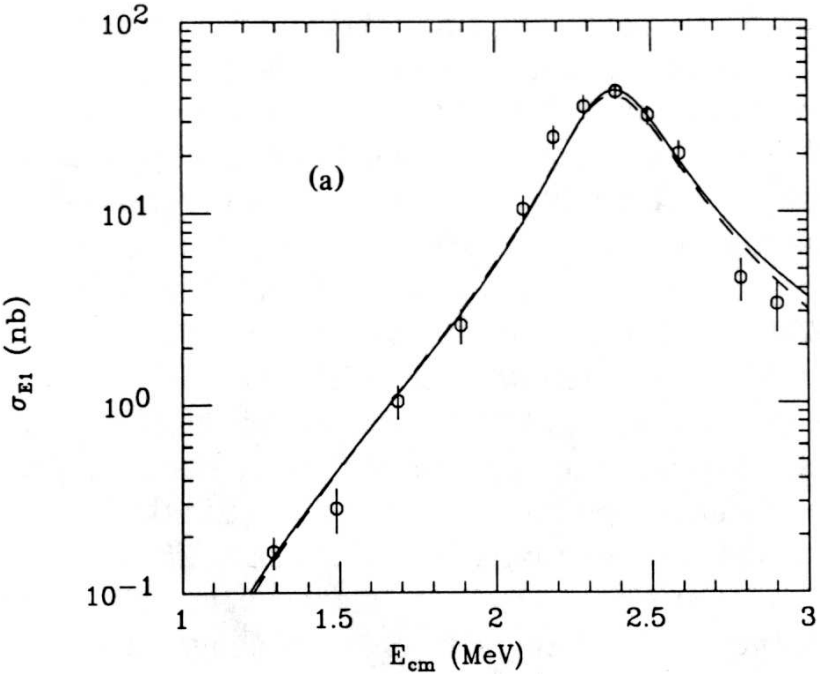

Fig. 23: The $^{12}C(\alpha,\gamma)^{16}O$ reaction cross section [30].

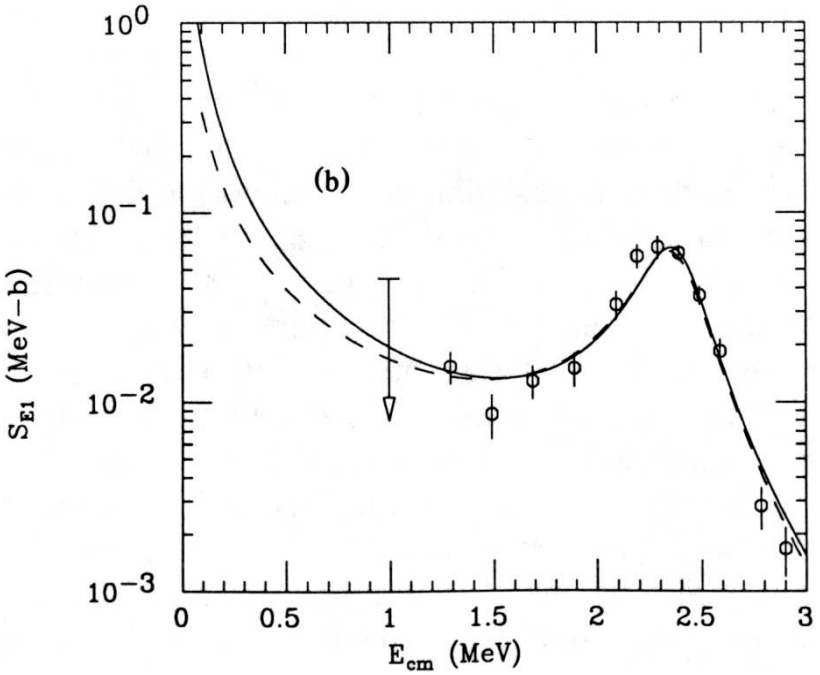

Fig. 24: Measured S - factor(s) for $^{12}C(\alpha,\gamma)^{16}O$ from [60].

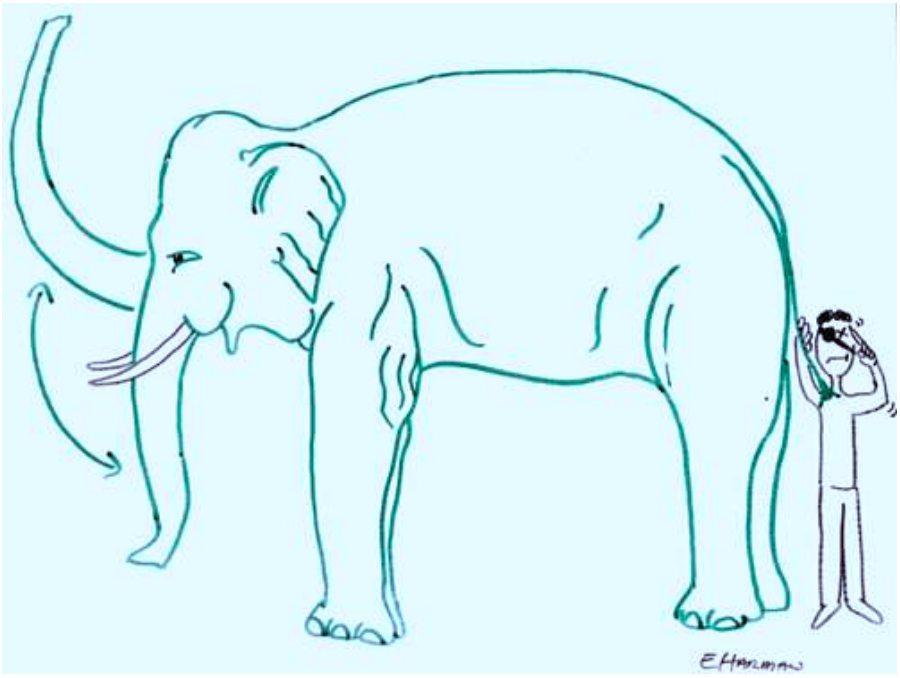

Fig. 25: A mythical blind man attempting to describe the position of the elephant's trunk by holding its tail (artwork by Eric T. Harman).

5 POSSIBLE SOLUTIONS [WITH SECONDARY OR RADIOACTIVE BEAMS]

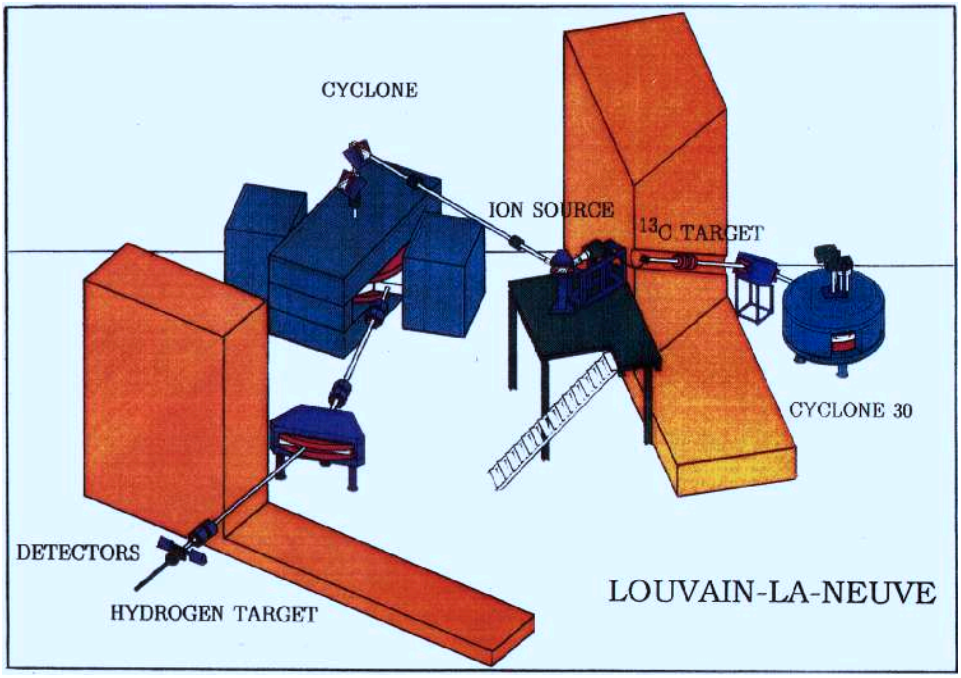

Fig. 26: The Louvain-La-Neuve Radioactive Beam Facility.

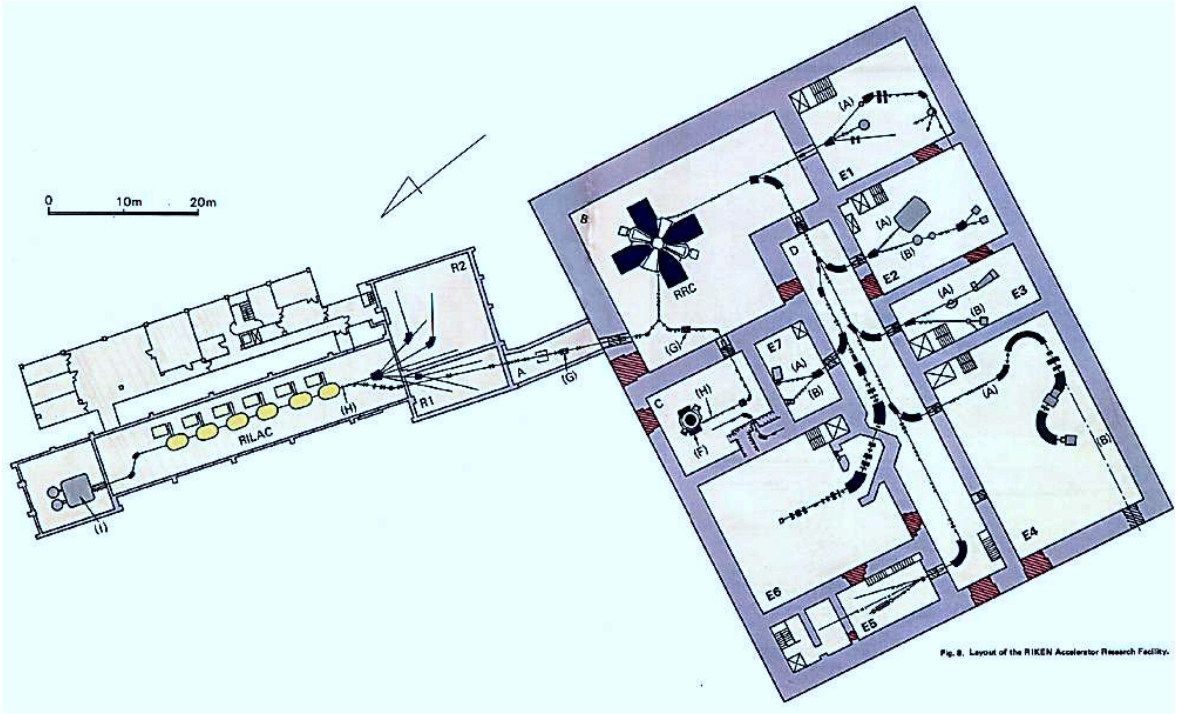

Fig. 27: The Riken-RIPS facility and the setup used for the Coulomb Dissociation of ^8B, the Rikkyo-Riken-Yale-Tokyo-Tsukuba-LLN collaboration [95].

In the previous chapter we have already described great advances made with the use of radioactive beams to study the $^{13}N(p,\gamma)^{14}O$ and the hot-CNO cycle, see Fig. 22. These studies were performed at the Louvain-La-Neuve (LLN) Radioactive beam facility with ^{13}N radioactive beams [92] and with ^{14}O radioactive beams at Riken [93] and at Ganil [94]. While the facility at LLN uses an ISOL type source and works at low energies, see Fig. 26, the facility at Riken, see Fig. 27, as well as that at Michigan State University, see Fig. 28, use high energy beams from fragmentation process.

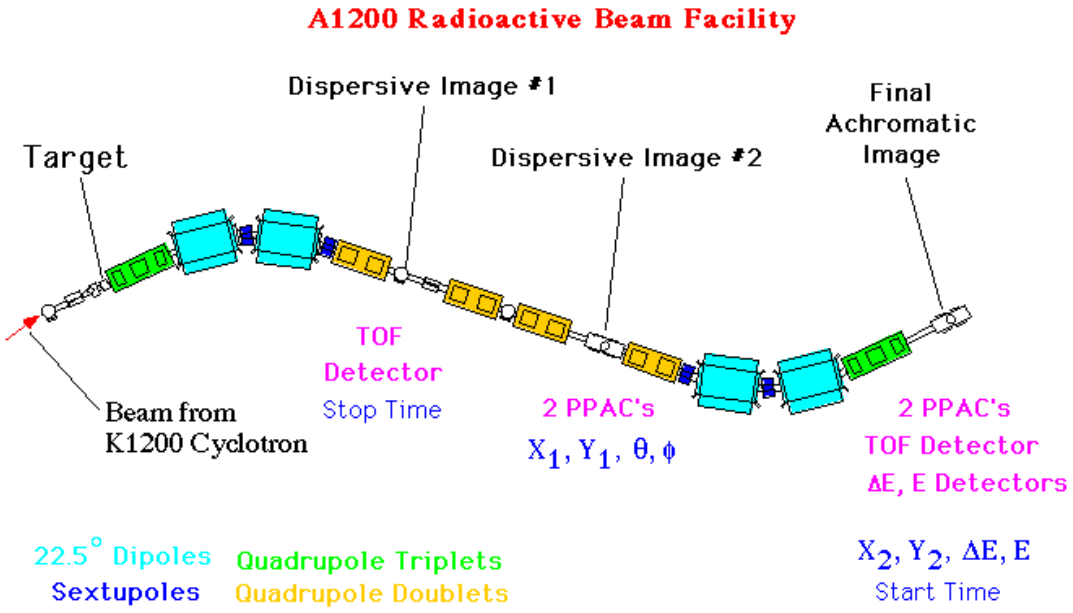

Fig. 28: The Michigan State University A1200 RNB facility.

5.1 The p-wave S-factor of $^{12}C(\alpha,\gamma)^{16}O$ from the beta-delayed alpha-particle emission of ^{16}N, Facts and Fallacies

The beta-delayed alpha-particle emission of ^{16}N may allow us to study the $^{12}C(\alpha,\gamma)^{16}O$ reaction in its time reverse fashion, the disintegration of ^{16}O to $\alpha + {}^{12}C$, and it provides a high sensitivity for measuring low energy alpha-particles and the reduced (virtual) alpha-particle width of the bound 1^- state in ^{16}O at 7.12 MeV, see Fig. 14. As shown in Fig. 29, low energy alpha-particle emitted from ^{16}N correspond to high energy beta's and thus to a larger phase space and enhancement proportional to the total energy to approximately the fifth power. In addition the apparent larger matrix element of the beta decay to the bound 1^- state provides further sensitivity to that state.

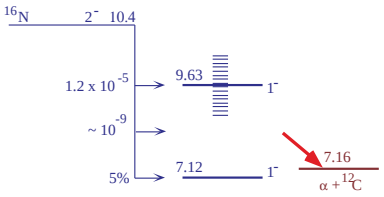

Fig. 29: Nuclear States involved in the beta-delayed alpha-particle emission of ^{16}N.

However, in this case one needs to measure the beta decay, see below, with a sensitivity for a branching ratio of the order of 10^{-9} or better. Prediction of the shape of the spectra of delayed alpha-particles from ^{16}N were first published by Baye and Descouvemont [96], see Fig. 30. Note the anomalous interference structure predicted to occur around 1.1 MeV, at a branching ratio at the level of 10^{-9}. The previously measured beta-delayed alpha-particle emission of ^{16}N [97] was analyzed using R-matrix theory by Barker [98] and lately by Ji, Filippone, Humblet and Koonin [99]. They conclude that the data measured at higher energies is dominated by the quasi bound state in ^{16}O at 9.63 MeV, see Fig. 14, and shows little sensitivity to the interference with the bound 1^- state. The data measured at low energies is predicted to have large sensitivity to the anomalous interference with the bound 1- state. Similar prediction were also given by a K-matrix analysis of Humblet, Filippone, and Koonin [100] of the same early data on ^{16}N [97]. However, it is clear that the interference phase measured in the beta-delayed alpha-particle emission of ^{16}N is not necessarily related to the one measured in $^{12}C(\alpha,\gamma)^{16}O$. Hence, a-priori we might already conclude that while the data on ^{16}N may prove useful for extracting the reduced alpha-width of bound 1^- state, it may be more difficult to exract from it the E1 astrophysical cross section factor.

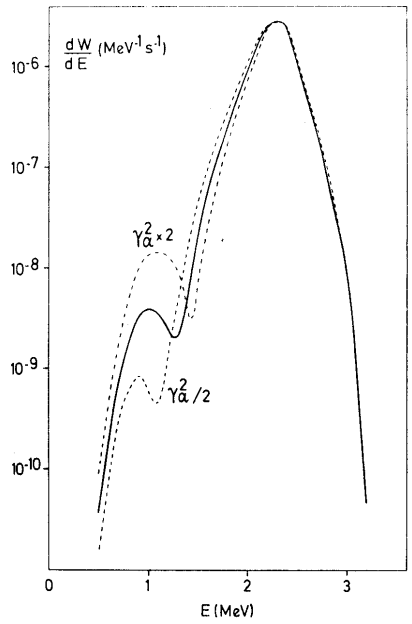

Fig. 30: Spectrum of the beta-delayed alpha-particle emission of ^{16}N, predicted by Baye and Descouvemont [96], some five years before the observation of the interference anomaly [55, 56, 62].

As shown in Fig. 29, the beta decay can only measure the p-wave S-factor of the $^{12}C(\alpha,\gamma)^{16}O$ reaction, and it also includes (small) contribution from an f-wave. The contribution of the f-wave have to be determined empirically and appears to be very small and leads to additional uncertainty in the quoted S-factor [55, 56]. The extraction of the total S- factor of the $^{12}C(\alpha,\gamma)^{16}O$ reaction could then be performed from the knowledge of the E2/E1 ratio which is better known then the individual quantities. An experimental program to study the beta-delayed alpha-particle emissionof ^{16}N (and other nuclei) was carried out at Yale [55, 56] and at TRIUMF [62]. From an R-matrix analysis the TRIUMF collaboration quoted a value for the p-wave astrophysical cross section factor of 79 $\pm$ 21 [101]. The Yale study was continued [63, 64] and it was found to be inconsistent with the TRIUMF result [62, 101], see Fig. 31. In contrast to the rather small error bar quoted by the TRIUMF collaboration ($\pm$20%) an R-matrix analyses of the data by Gerry Hale [65] showed that the ^{16}N data does not rule out a small S-factor. We conclude that the p-wave S-factor for the $^{12}C(\alpha,\gamma)^{16}O$ reaction is in fact not known with the accuracy claimed by Buchmann *et al.* [62] and Azuma *et al.* [101]. In order to determine both the p- and d- wave S-factors of the $^{12}C(\alpha,\gamma)^{16}O$ one can not resort to indirect measurements such the beta-delayed alpha-particle emission of ^{16}N and one must measure the cross section of the $^{12}C(\alpha,\gamma)^{16}O$ reaction at energies as low as possible. In the next section we discuss such a possibility using a new High Intensity Gamma Source (HIGS) at TUNL/Duke.

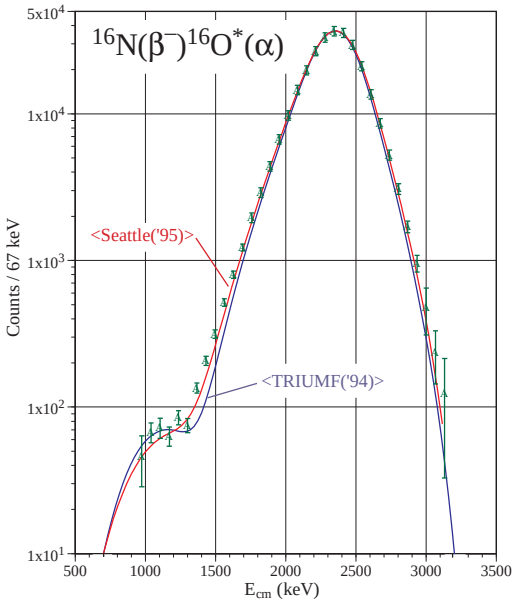

Fig. 31: The newly measured Spectrum of the beta-delayed alpha-particle emission of ^{16}N [63, 64] that appears consistent with the unpublished data of the Seattle group, but disagrees with the TRIUMF data [101].

5.2 The Duke/TUNL Experiment: $^{16}O(\gamma,\alpha)^{12}C$

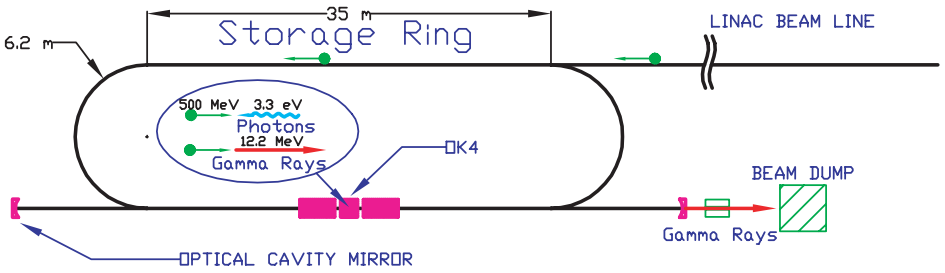

Fig. 32: The electron ring of the Duke High Intensity Gamma Source (HIGS) [102].

For determination of the cross section of the $^{12}C(\alpha,\gamma)^{16}O$ at very low energies, as low as $E_{cm} = 700$ KeV, considerably lower than measured till now, it is very useful to have an experimental setup with three conditions: an amplified cross section, high luminosity and low background. It turns out that the use of the inverse process, the $^{16}O(\gamma,\alpha)^{12}C$ reaction may indeed satisfy all three conditions. The cross section of $^{16}O(\gamma,\alpha)^{12}C$ reaction (with polarized photons) at the kinematical region of interest (photons approx 8-8.5 MeV) is larger by a factor of 50 than the cross section of the

direct $^{12}C(\alpha,\gamma)^{16}O$ reaction that occurs in for example Red Giants. Note that the polarization yield an extra factor of two in the enhancement. Thus for the lowest data point measured at 0.9 MeV with the direct cross secion of approx. 60 pb, the photodissociation cross section is 3 nb. It is evident that with similar luminosities, see below, and similar or lower background, the photodissociation cross section can be measured yet to even lower equivalent energies, as low as 0.7 MeV, where the direct $^{12}C(\alpha,\gamma)^{16}O$ cross section is predicted to be of the order of 1 pb. It is clear that detailed balance aids a great deal in this case for measuring the $^{12}C(\alpha,\gamma)^{16}O$ at yet lower energies. However, with (secondary photons from HIGS, see Fig. 32) one can not observe cascade gamma decay, which are considered to be small at low energies.

The luminosity using for example a 100 cm long target of the gas CO_2 at a pressure of 76 torrs (100 mbar), and with a photon beams of 2×10^9 /sec, we obtain a luminosity of $10^{30}\ sec^{-1}cm^{-2}$, or a day long integrated luminosity of $0.1pb^{-1}$. Hence a measurement of the photodissociation of ^{16}O with cross section of 10 pb, with a high efficiency detector would yield one count per day. We conclude that it is conceivable that a facility with such luminosity and low background together with a high efficiency detector may allow us to measure the photodissociation cross section to a few tens of pb and thus as low as several hundreds of fb for the direct $^{12}C(\alpha,\gamma)^{16}O$ reaction.

The High Intensity Gamma Source (HIGS) [102], in the process of being funded by the USDOE at TUNL/Duke, has already achieved many of its mile stones and it is rapidly approaching its design goal of 2-200 MeV gammas, with 9 MeV gammas at a resolution of 0.1% and intensity in the 10^9 /sec range. The schematical layout of the HIGS facility is shown in Fig. 32. With a 500 MeV pulsed electron beam circulating in the ring, it passes an undulator (OK4) that produces Free Electron Laser photons of 3.3 eV. These photons are reflected back in an optical cavity and arrive in phase for the next pulse in the ring, due to the lasing action. The backscattered photons (of 12.2 MeV) are collimated and used for nuclear physics research at a designated Hall, where we plan to set our experiment. With a Q value of -7.162, our experiment will utilize gammas of energies ranging from 8 to 10 MeV. Note that the emitted photons are linearly polarized [103] and the emitted particles are in a horizontal plane. This simplifies the tracking of particles in this experiment. In addition as the beam is a pulsed, one may use the time information in the trigger of the experiment as well as for using time of flight techniques to further reduce the background.

The main background in such a photodissociation experiment appears to be the large flux of Compton electrons. A promissing detection system would involve the construction of a Time Projection Chamber (TPC). Since the range of available alphas is approximately 8 cm the TPC will be 20 cm wide and one meter long.

The TPC could be constructed to be largely insensitive to single Compton electrons, but allow to track both alphas and carbons emitted almost back to back in time correlation. The very different range of alphas and carbons (approx. a factor of 4) aids in the particle identification. Such a TPC detector also allows to measure angular distributions with respect to the polarization vector of the photon, and thus seperate the E1 and E2 components of the $^{12}C(\alpha,\gamma)^{16}O$ reaction.

5.3 The Coulomb dissociation of ^{14}O (hot CNO) and ^{8}B (solar neutrino's):

The Coulomb Dissociation [104] Primakoff [105] process, is the time reverse process of the radiative capture. In this case instead of studying for example the fusion of a proton plus a nucleus (A-1), one studies the disintegration of the final nucleus (A) in the Coulomb field to a proton plus the (A-1) nucleus. The reaction is made possible by the absorption of a virtual photon from the field of a high Z nucleus such as ^{208}Pb. In this case since $\frac{\pi}{k^2}$ for a photon is approximately 1000 times larger than that of a particle beam, the small cross section is enhanced. The large virtual photon flux (typically 100-1000 photons per collision) also gives rise to enhancement of the cross section. Our understanding of the Coulomb Excitation and the virtual photon flux allow us (as in the case of electron scattering) to deduce the inverse nuclear process. However in Coulomb Dissociation since αZ approaches unity (unlike the case in electron scattering), higher order Coulomb effects (Coulomb Post Acceleration) may be non-negligible and they need to be understood [106]. The success of the experiment is in fact hinging on understanding such effects and designing the kinematical conditions so as to minimize such effects.

Hence the Coulomb Dissociation process has to be measured with great care with kinematical conditions carefully adjusted so as to minimize nuclear interactions (i.e. distance of closest approach considerably larger then 20 fm, hence very small forward angles scattering), and measurements must be carried out at high enough energies (many tens of MeV/u) so as to maximize the virtual photon flux [107]. Indeed when such conditions are not carefully selected [108] the measured cross section was shown to be dominated by nuclear effects [109, 110], which can not be reliably calculated to allow the extraction of the inverse radiative capture cross section.

Good agreement between measured cross section of radiative capture through a nuclear state, or in the continuum, was achieved for the Coulomb Dissociation of ^{6}Li and the $d(\alpha,\gamma)^{6}Li$ capture reaction [111], and the Coulomb Dissociation of ^{14}O and the $p(^{13}N,\gamma)^{14}O$ capture reaction [92, 93, 94]. In addition we note that test

experiment on the Coulomb Dissociation of ^{13}N [93] was also found to be in agreement with the $^{12}C(p,\gamma)^{13}N$ capture reaction.

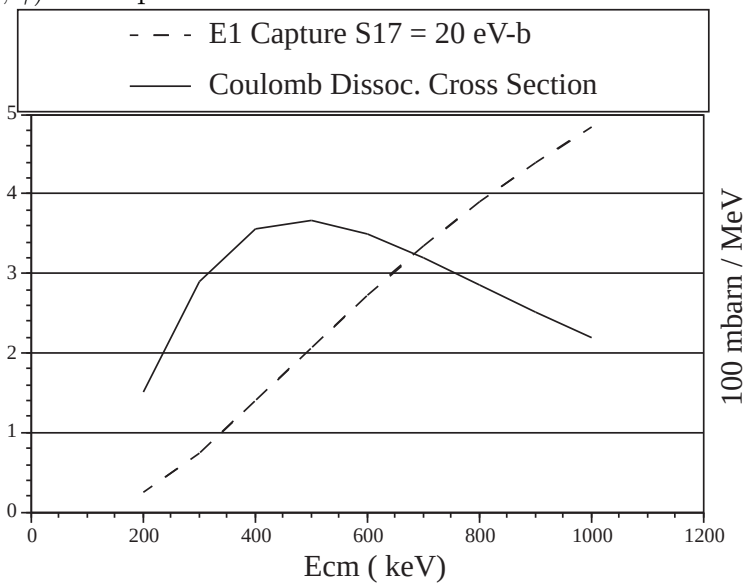

Fig. 33: The cross section for Coulomb Dissociation and E1 capture.

The Coulomb Dissociation of ^{8}B may provide a good opportunity for resolving the issue of the absolute value of the cross section of the $^{7}Be(p,\gamma)^{8}B$ reaction, see chapter 4. The Coulomb Dissociation yield arise from the convolution of the inverse nuclear cross section times the virtual photon flux. While the first one is decreasing as one approaches low energies, the second one is increasing (due to the small threshold of 137 keV). Hence as can be seen in Fig. 33, over the energy region of 400 to 800 keV the predicted measured yield is roughly constant. This is in great contrast to the case of the nuclear cross section that is dropping very fast at low energies, see Fig. 33. Hence measurements at these energies could be used to evaluate the absolute value of the cross section.

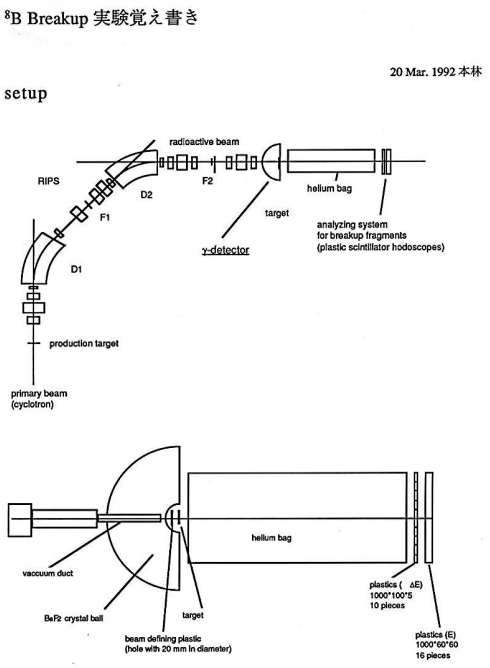

Fig. 34: The experimental setup of the RIKEN Experiments.[95, 112, 113]

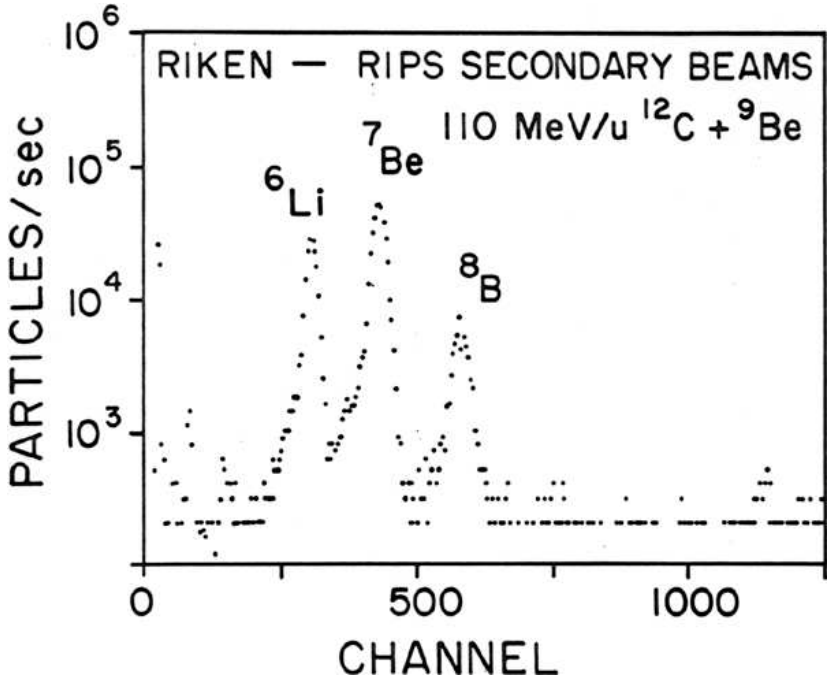

Fig. 35: Radioactive beams extracted from the Riken-RIPS facility and used in the study of the Coulomb Dissociation of ^8B, a Rikkyo-Riken-Yale-Tokyo-Tsukuba-LLN collaboration [95].

An experiment to study the Coulomb Dissociation of ^8B was performed during March-April, 1992, at the Riken radioactive beam facility, using the setup shown in Fig. 34. The radioactive beams extracted from the RIPS separator, see Fig. 27, are shown in Fig. 35. Indeed the results of the experiment allow us to measure the

radiative capture $^7Be(p,\gamma)^8B$ cross section and the results of the RIKEN I [95] and the RIKEN II [112, 113] are consistent with the absolute value of the cross section measured by Filippone et al. [73] and by Vaughn et al. [76], as shown in Fig. 36. This experiment was continued at GSI [114] with similar results at low energy. The results of the RIKEN I [95], RIKEN II [112, 113], GSI [114] as well as the MSU result on the E2/E1 [116] are shown in Table II. Note the MSU data suggest an E2 larger than expected from RIKEN I data [115], RIKEN II [112], and GSI data [114].

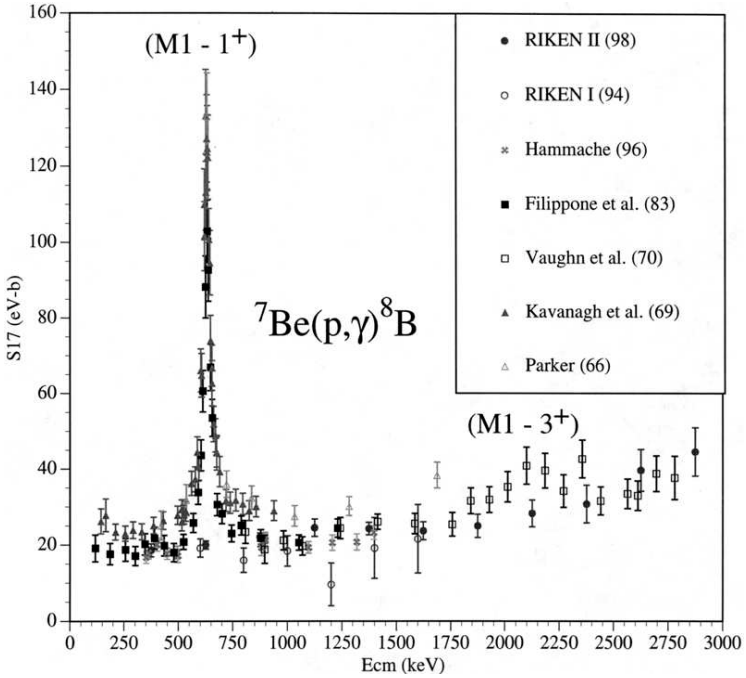

Fig. 36: Extracted $S_17(E)$ cross section factors by the RIKEN experiments as compared to direct measurements.

Table II: Measured S-factors in Coulomb dissociation experiments.

Experiment	$S_{17}(0)$ eV-b	$S_{E2}/S_{E1}(0.6$ MeV)
RIKEN1 [95]	16.9 ± 3.2	$< 7 \times 10^{-4}$ [115]
RIKEN2 [112]	18.9 ± 1.8	$< 4 \times 10^{-5}$ [113]
GSI1 [114]	$20.6 \pm 1.2 \pm 1.0$	$< 3 \times 10^{-5}$
MSU [116]		$6.7\ +2.8\ -1.9 \times 10^{-4}$
ADOPTED	19.4 ± 1.3	$< 3 \times 10^{-5}$

5.4 The $^7Be(p,\gamma)^8B$ Reaction Studies With ^7Be Radioactive Beams at LLN:

An experiment to study the $^7Be(p,\gamma)^8B$ reaction with ^7Be radioactive beam is in progress, a UConn-LLN collaboration at LLN [117, 118] The experimental detector setup for the UConn-LLN experiment is shown in Fig. 37. The recoil ^8B emerge with a (step) distribution of energies with widths approximately 0.7 MeV, and a stopping spread in aluminum of approximately 0.5 μm. Thus the stopped ^8B are designed to be equally spread over the two aluminum catcher foils (0.5 μm each). The beta-delayed alpha-particle emission of ^8B is measured by measuring coincidence between the two back to back equal energy alpha-particles detected in a pair of detectors, see fig. 37.

In the target region, two monitors measure beam intensity by measuring the elastic scattering off a thin Au foil (evaporated onto a very thin carbon backing) and the recoil protons off the target. The cross section of the $^7Be(p,\gamma)^8B$ reaction will be measured relative to the elastic scattering, thereby removing several systematic uncertainties related to beam-target composition. The hydrogen component of the target is continuously monitored by measuring the recoil protons from the target.

Since two alpha-particles are associated with every decay we calculated a very-large detection efficiency, approximately 50% of 2π. Our extensive Monte carlo simulations yield a large (98%) coincidence efficiency, and thus approximately 50% total coincidence efficiency for two equal energy correlated back to back alpha-particles. For a ^8B transfer time of 0.07 sec, every 0.5 sec, we obtain a total alpha-particle detection efficiency of approximately 25%. The closed detection geometry (50% of 4π) with a front and back detectors (a-la calorimetry style) also ensures that the total alpha detection efficiency is nearly independent of the exact location of the collection foils, as long as the two foils remain parallel and at constant distance and the recoil ^8B nuclei are spread equally on both catcher foils.

A beam intensity of 5×10^8 $/sec$ and a 250 $\mu g/cm^2$ CH_2 target ($\Delta E_{cm} =$ 100 keV) containing 2×10^{19} $hydrogens/cm^2$ yield a luminosity of 10^{28} $/sec/cm^2$. With expected cross sections of $\sigma = 0.5,\ 0.4$ and 0.2 μb, at $E_{cm} = 1.0,\ 0.8$ and 0.5 MeV, respectively, and alpha-particle detection efficiency of 25%, we obtain count rates of approximately 5, 4, and 2 counts per hour. Thus experiments lasting two to three days at $E_{cm} = 1.0,\ 0.8$ and 0.5 MeV, respectively, will yield a total count of 240, 192 and 144 counts and statistical uncertainties of 6.4%, 7.2% and 8.3%, respectively. With approved 9 days of experiment we plan to adjust the length of runs to achieve 5% precision at each data point.

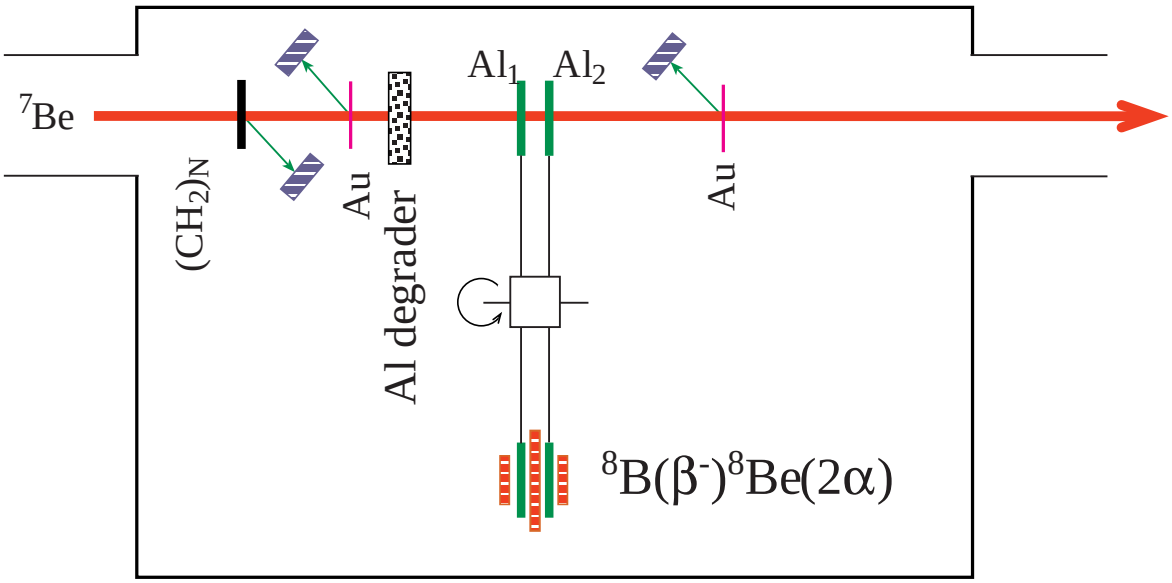

Fig. 37: The Setup of the LLN experiment [117, 118].

6 Conclusions and Acknowledgements

We conclude that radioactive beams could be used for carefully planned experiments to solve some of the outstanding and most important problems of nuclear astrophysics today, and hence promise a rich future for low energy nuclear astrophysics studies.

I would like to acknowledge the help of Ralph France III in preparing this manuscript and the work of N. Iwasa, T. Kikuchi, K. Suemmerer, F. Boue and P. Senger on the data analyses of the CD data and Ralph H. France III and James E. McDonald on the data analysis of the $^7Be(p,\gamma)^8B$ reaction. I also acknowledge discussions and encouragements from Professors J.N. Bahcall, C.A. Bertulani, G. Baur, and Th. Delbar.

References

[1] Dorrit Hoffleit, Yale Alumni Magazine, Nov.(1985)28.

[2] D.C. Wang, and S.M. Gong, The historical records of Halley's comet in China, Earth, Moon, and Planets, David Reidel Publ. comp. **34**(1986)55.

[3] Donald D. Clayton, Principles of Stellar Evolution and Nucleosynthesis, University of Chicago Press, 1968.

[4] C.E. Rolfs, and W.S. Rodney; Cauldrons in the Cosmos, University of Chicago Press, 1988.

[5] Gordon Baym, Lectures on Quantum Mechanics, W.A. Benjamin, Inc., 1969, p. 431.

[6] John N. Bahcall, Neutrino Astrophysics, Cambridge Univ. Press, 1989.

[7] Hans A. Bethe, Physics Today, **21:9**(1968)36.

[8] P.R. Demarque, J.R. Percy, ApJ **140**(1964)541.

[9] S. Chandrasekhar, Rev. Mod. Phys. **56**(1984)137.

[10] P. Demardue, C.P. Deliyannis, and E. Sarajendini, Observation Tests of Cosmological Inflation, Eds. T. Shank et al., Cluwer Acad. Press, Netherlands, 1991, p. 111.

[11] David N. Schramm and Robert V. Wagoner, Ann. Rev. Nucl. Sci. **27**(1977)37.

[12] Ann Merchant Boesgaard and Gary Steigman; Ann. Rev. Astron. Astrophy. **23**(1985)319.

[13] R. Rebolo, P. Molaro, and J.F. Beckman, Astron. Astrop. **192**(1988)192.

[14] David N. Schramm, private communication, 1992.

[15] A.G. Riess *et al.*; Astr. Jour. **116,3**(1998)1009.

[16] E.P. Hubble, Silliman Lectures, Yale University, 1936.

[17] A.A. penzias and R.W. Wilson; ApJ. **142**(1965)419.

[18] R.H. Dicke, P.J.E. Peebles, P.G. Roll, and D.T. Wilkinson; ApJ. **142**(1965)414.

[19] J.H. Applegate, and C.J. Hogan; Phys. Rev. **D31**(1985)3037.

[20] J.H. Applegate, C.J. Hogan, and R.J. Scherrer; Phys. Rev. **D35**(1987)1151.

[21] J.H. Applegate, C.J. Hogan, and R.J. Scherrer; ApJ. **329**(1988)572.

[22] C.R. Alcock, G.M. Fuller, and G.J. Mathews, ApJ. **320**(1987)439.

[23] R.A. Malaney, and W.A. Fowler; ApJ. **333**(1988)14.

[24] R.N. Boyd, and T. Kajino; ApJ. **336**(1989)L55.

[25] C.R. Alcock, D.S. Dearborn, G.M. Fuller, G.J. Mathews, and B.S. Meyer; Phys. Rev. Lett. **64**(1990)2607.

[26] Moshe Gai, Phys. Rev., RC, **C45**(1992)2548.

[27] F.R. Brown, F.P. Butler, H. Chen, N.H. Christ, Z. Dong, W. Schaffer, L.I. Unger, and A. Vaccarino; Phys. Rev. Lett. **65**(1990)2491.

[28] S.G. Ryan, J.E. Norris, M.S. Bessell, and C.P. Deliyannis; ApJ. **388**(1992).

[29] T.P. Walker, G.J. Mathews, and V.E. Viola; ApJ. **299**(1985)745.

[30] W.A. Fowler, Rev. Mod. Phys. **56**(1984)149.

[31] G.R. Caughlan, and W.A. Fowler, At. Data Nucl. Data Tables **40**(1988)283.

[32] F.C. Barker, and T. Kajino; Proc. Int. Workshop on Unstable Beams in Astrophysics, Tokyo, 7-8 June, 1991, World Scientific, Singapore, 1992, p. 63

[33] W.A. Fowler, G.R. Caughlan, and B.A. Zimmerman, Ann. Rev. Astron. and Ap. **5**(1967)525.

[34] W.A. Fowler, G.R. Caughlan, and B.A. Zimmerman, Ann. Rev. Astron and Ap. **13**(1975)69.

[35] P.B. Fernandez, E.G. Adelberger, and A. Garcia, Phys. Rev. **C89**(1989)1887.

[36] Yoram Alhassid, Moshe Gai, and George F. Bertsch; Phys. Rev. Lett. **49**(1982)1482.

[37] J.N. Bahcall, and R.K. Ulrich, Rev. Mod. Phys. **60**(1988)297.

[38] J.N. Bahcall, and M.H. Pinsonneault; Rev. Mod. Phys. **64**(1992)885.

[39] S. Turck-Chieze, S. Cahen, M. Casse, and C. Doom, ApJ **335**(1988)415.

[40] Sylvaine Turck-Chieze, and Ilidio Lopes; ApJ. **408**(1993)347.

[41] S. Turck-Chieze, W. Dappen, E. Fossat, J. Provost, E. Schatzman, and D. Vignaud; Phys. Rep. **230**(1993)57.

[42] K.S. Hirata et al. Phys. Rev. Lett. **65**(1990)1297.

[43] K. Inoue for the Kamiokande III collaboration, XXVIIIth Recontre de Moriond, Les Arcs, Savoi, France, March 13-20, 1993.

[44] Y. Fukuda *at al.*; Phys. Rev. Lett. **81**(1998)1158.

[45] A.I. Abazov et al. Phys. Rev. Lett. **67**(1991)3332.

[46] P. Anselmann et al. Phys. Lett. B314(1993)445, ibid GX 44-1994, February, 1994, submitted to Phys. Lett. B.

[47] G.T. Ewan, W.F. Davidson, C.G. Hargrove, Phys. in Canada **48**(1992)112.

[48] A.B. McDonald, Phys. in Canada **48**(1992)120.

[49] J. Boger et al.; nucl-ex/9910016, to be published, 1999.

[50] L. Wolfenstein, Phys. Rev. **D17**(1978)2369, ibid **D20**(1979)2634.

[51] S.P. Mikheyev, and A.Yu. Smirnov, Yad. Fiz. **44**(1985)847 [Sov. J. Nucl. Phys. **42**(1985)913].

[52] Peter D. Parker, Proc. fifth Int. Conf. Clust. Nucl., Kyoto, 1988, J. Phys. Soc. Jpn. **58**(1989)Suppl. 196.

[53] H.M.J. Boffin, G. Paulus, M. Arnould, and N. Mowlavi; Astron. Astrophys. **279**(1993)173.

[54] B.G. Levi, Physics Today, Search and Discovery, July, 1993, p. 23.

[55] Z. Zhao, R.H. France III, K.S. Lai, S.L. Rugari, M. Gai, and E.L. Wilds, Phys. Rev. Lett. **70**(1993)2066, ER **70**(1993)3524.

[56] Z. Zhao, Ph.D. thesis, Yale University, 1993.

[57] P. Dyer and C.A. Barnes; Nucl. Phys. **A233**(1974)495.

[58] K.U. Kettner *et al.*; Z. Phys. **A308**(1982)73.

[59] A. Redder *et al.*; Nucl. Phys. **462**(1987)385.

[60] R.M. Kremer *et al.*; Phys. rev. Lett. **60**(1988)1475.

[61] J.M.L. Ouellet *et al.*; Phys. Rev. Lett. **69**(1992)1896, data changed in a later publication, ibid, Phys. Rev. **C54**(1994)1982.

[62] L. Buchmann, R.E Azuma, C.A. Barnes, J.M. D'Auria, M. Dombsky, U. Giesen, K.P. Jackson, J.D. King, R.G. Korteling, J. Powell, G. Roy, J. Vincent, T.R. Wang, S.S.M. Wong, and P.R. Wrean; Phys. Rev. Lett. **70**(1993)726.

[63] R.H. France III, E.L. Wilds, N.B. Jevtic, J.E. McDonald, and M. Gai; Nucl. Phys. **A621**(1997)165c.

[64] R.H. France III; Ph.D. thesis, Yale University, 1996.

[65] G.M. Hale; Nucl. Phys. bf A621(1997)177c.

[66] I. Iben; ApJ. **196**(1975)525, ibid **196**(1975)549.

[67] T.A. Weaver and S.E. Woosley; Ann. NY Acad. Sci. **336**(1980)335.

[68] Xi Ze-zong, Po Shu-jen [translated by K.S. Yang]; Science **154**(1966)597.

[69] Jewan Kim, Barley existing things, Mineum Publishing company, 1993, Seoul, Korea.

[70] T.A. Weaver, and S.E. Woosley; Phys. Rep. **227**(1993)65.

[71] F.C. Barker, and H.R. Spear, ApJ **307**(1986)847.

[72] C.W. Johnson, E. Kolbe, S.E. Koonin, and K. Langanke, ApJ **392**(1992)320.

[73] B.W. Filippone, A.J. Elwyn, C.N. Davis, and D.D. Koetke, Phys. Rev. Lett. **50**(1983)412, ibid Phys. Rev. **C28**(1983)2222.

[74] R.W. Kavanagh, T.A. Tombrello, J.M. Mosher, and D.R. Goosman, Bull. Amer. Phys. Soc. **14**(1969)1209.

[75] P.D. Parker; Phys. Rev. **150**(1966)851, ApJ **153**(1968)L85.

[76] F.J. Vaughn, R.A. Chalmers, D. Kohler, and L.F. Chase Jr; Phys. Rev. **C2**(1970)1657.

[77] E.G. Adelberger, S.A. Austin, J.N. Bahcall, A.B. Balantekin, G. Bertsch, G. Bogaert, L. Buchmann, F.E. Cecil, A.E. Champagne, L. de Braeckeleer, C.A. Duba, S.R. Elliott, S.J. Freedman, M. Gai, G. Goldring, C.R. Gould, A. Gruzinov, W.C. Haxton, K.M. Heeger, E. Henley, M. Kamionkowski, R.W. Kavanagh, S.E. Koonin, K. Kubodera, K. Langanke, T. Motobayashi, V. Pandharipande, P. Parker, R.G.H. Robertson, C. Rolfs, R. Sawyer, N. Shaviv, T.D. Shoppa, K. Snover, E. Swanson, R.E. Tribble, S. Turck-Chiez, J.F. Wilkerson.; Rev. of Modern Phys. **70**(1998)1265.

[78] F. Strieder et al., Eur. Phys. J. A3(1998)1.

[79] L. Weissman et al., Nuc. Phys. A630(1998)678.

[80] F. Hammache et al., Phys. Rev. Lett. 80(1998)928.

[81] M. Hass et al., Phys. Lett. B462(1999)237.

[82] A.Y. Zyuzin *et al.*; Nucl. Inst. Meth. **A438**(1999)109.

[83] B.K. Jennings, S. Karataglidis, and T.D. Shoppa, Phys. Rev. C **58** (1998) 3711.

[84] C.A. Barnes *et al.*; Phys. Lett. **197**(1987)315.

[85] P. Decrock et al.; Phys. Rev. **C48**(1993)2057.

[86] T.E. Chupp, R.T. Kozus, A.B. McDonald, P.D. Parker, T.F. Wang, and A.J. Howard, Phys. Rev. **C31**(1985)1023.

[87] T.F. Wang, Ph.D. thesis, Yale University, unpublished.

[88] P. Aguer et al., Proc. Int. Symp. Heavy Ions Phys. and Nucl. Astro., ed. S. Kubono, M. Ishihara, and T. Nomura, World Scie. 1989, p. 107.

[89] M.S. Smith et al., Phys. Rev. **C47**(1993)2740.

[90] M. Gell-Mann, and V.L. Telegdi, Phys. Rev. **91**(1953)169.

[91] L.A. Radicati, Phys. Rev. **87**(1952)521.

[92] P. Decrock, Th. Delbar, P. Duhamel, W. Galster, M. Huyse, P. Leleux, I. Licot, E. Lienard, P. Lipnik, M. Loiselet. C. Michotte, G. Ryckewaert, P. Van Duppen, J. Vanhorenbeeck, J. Vervier; Phys. Rev. Lett. **67**(1991)808.

[93] T. Motobayashi, T. Takei, S. Kox, C. Perrin, F. Merchez, D. Rebreyend, K. Ieki, H. Murakami, Y. Ando, N. Iwasa, M. Murokawa, S. Shirato, J. Ruan (Gen), T. Ichihara, T. Kubo, N. Inabe, A. Goto, S. Kubono, S. Shimoura, and M. Ishihara; Phys. Lett. **B264**(1991)259.

[94] J. Kiener, A. Lefebvre, P. Aguer, C.O. Bacri, R. Bimbot, G. Bogaert, B. Borderie, F. Calpier, A. Coe, D. Disidier, S. Fortier, C. Grunberg, L. Kraus, I. Linck, G. Pasquier, M.F. Rivet, F. St. Laurent, C. Stephan, L. Tassan-Got, and J.P. Thibaud; Nucl. Phys. **A552**(1993)66.

[95] T. Motobayashi, N. Iwasa, Y. Ando, M. Kurokawa, H. Murakami, J. Ruan (Gen), S. Shimoura, S. Shirato, N. Inabe, M. Ishihara, T. Kubo, Y. Watanabe, M. Gai, R.H. France III, K.I. Hahn, Z. Zhao, T. Nakamura, T. Teranishi, Y. Futami, K. Furataka, and T. Delbar; Phys. Rev. Lett. **73**(1994)2680.

[96] D. Baye, and P. Descouvemont; Nucl. Phys. **A481**(1988)445.

[97] K. Neubeck, H. Schober, and H. Waffler; Phys. Rev. **C10**(1974)320.

[98] F.C. Barker; Aust. Jour. Phys. **24**(1971)777.

[99] X. Ji, B.W. Filippone, J. Humblet, and S.E. Koonin; Phys. Rev. **C41**(1990)1736.

[100] J. Humblet, B.W. Filippone, and S.E. Koonin; Phys. Rev. **C44**(1991)2530.

[101] R.E. Azuma, *et al.* Phys. Rev. C50(1994)1194.

[102] A Proposal: "A FREE-ELECTRON LASER GENERATED GAMMA-RAY BEAM FOR NUCLEAR PHYSICS", W. Tornow, R. Walter, H.R. Weller, V. Litvinenko, B. Mueller, P. Kibrough, Duke/TUNL, 1997.

[103] V.N. Litvinenko et al., Phys. Rev. Letts. **78**(1997)4569.

[104] G. Baur, C.A. Bertulani, and H. Rebel; Nucl. Phys. **A458**(1986)188.

[105] H. Primakoff; Phys. Rev. **81**(1951)899.

[106] H. Esbensen and G.F. Bertsch; Phys. Lett. **B359**(1995)13 ibid 531 Nucl. Phys. **A600**(1996)37.

[107] J.D. Jackson, Classical Electromag., John Wiley, New York, 1962, Ch. 14.

[108] J. von Schwarzenberg *et al.*; Phys. Rev. **C53**(1996)R2598.

[109] F.M. Nunes, and I.J. Thompson; Phys. Rev. **C57**(1998)R2818.

[110] C.H. Dasso, S.M. Lenzi, and A. Vitturi; nucl-th/9806002, to be published.

[111] J. Kiener, H.J. Gils, H. Rebel, S. Zagromski, G. Gsottschneider, N. Heide, H. Jelitto, and J. Wentz; Phys. Rev. **C44**(1991)2195.

[112] T. Kikuchi, T. Motobayashi, N. Iwasa, Y. Ando, M. Kurokawa, S. Moriya, H. Murakami, T. Nishio, J. Ruan (Gen), S. Shirato, S. Shimoura, T. Uchibori, Y. Yanagisawa, M. Ishihara, T. Kubo, Y. Watanabe, M. Hirai, T. Nakamura, H. Sakurai, T. Teranishi, S. Kubono, M. Gai, R.H. France III, K.I. Hahn, Th. Delbar, C. Michotte, and P. Lipnik; Phys. Lett. **B391**(1997)261.

[113] T. Kikuchi, T. Motobayashi, N. Iwasa, Y. Ando, M. Kurokawa,, S. Moriya, H. Murakami, T. Nishio, J. Ruan (Gen), S. Shirato, S. Shimoura, T. Uchibori, Y. Yanagisawa, H. Sakurai, T. Teranishi, Y. Watanabe, M. Ishihara, M. Hirai, T. Nakamura, S. Kubono, M. Gai, R.H. France III, K.I. Hahn, Th. Delbar,P. Lipnik, and C. Michotte. Eur. Phys. J. **A3**(1998)213.

[114] N. Iwasa, F. Boue, G. Surowka, K. Summerer, T. Baumann, B. Blank, S. Czajkowski, A. Forster, M. Gai, H. Geissel, E. Grosse, M. Hellstrom, P. Koczon, B. Kohlmeyer, R. Kulessa, F. Laue, C. Marchand, T. Motobayashi, H. Oeschler, A. Ozawa, M.S. Pravikoff, E. Schwab, W. Schwab, P. Senger, J. Speer, C. Sturm, A. Surowiec, T. Teranishi, F. Uhlig, A. Wagner, W. Walus, and C.A. Bertulani; Phys. Rev. Lett. **83**(1999)2910.

[115] Moshe Gai, and Carlos A. Bertulani; Phys. Rev. **C52**(1995)1706.

[116] B. Davids *et al.*, Phys. Rev. Lett. **81**(1998)2209.

[117] M. Gai, J.E. McDonald, R.H. France III, J.S. Schweitzer, C. Angulo, Ch. Barue, S. Cherubini, M. Cogneau, Th. Delbar, M. Gaelens, P. Leleux, M. Loiselet, A. Ninane, G. Ryckewaert, K.B. Swartz, D. Visser. Bull. Amer. Phys. Soc. **44,II**(1999)1529.

[118] J.E. McDonald; Ph.D. thesis, University of Connecticut, 2000.